A generalized model of pelagic biogeochemistry for the global ocean ecosystem. Part II: numerical simulations.

M. Vichi * S. Masina A. Navarra

Istituto Nazionale di Geofisica e Vulcanologia, Sezione di Bologna, Italy

Abstract

This paper presents a global ocean implementation of a multi-component model of marine pelagic biogeochemistry coupled on-line with an ocean general circulation model forced with climatological surface fields (PELAgic biogeochemistry for Global Ocean Simulations, PELAGOS). The final objective is the inclusion of this model as a component in an Earth System model for climate studies. The pelagic model is based on a functional stoichiometric representation of marine biogeochemical cycles and allows simulating the dynamics of C, N, P, Si, O and Fe taking into account the variation of their elemental ratios in the functional groups. The model also includes a parameterization of variable chlorophyll:carbon ratio in phytoplankton, carrying chl as a prognostic variable. The first part of the paper analyzes the contribution of non-local advective-diffusive terms and local vertical processes to the simulated chl distributions. The comparison of the three experiments shows that the mean chl distribution at higher latitudes is largely determined by mixing processes, while vertical advection dominates the distribution in the equatorial upwelling regions. Horizontal advective and diffusive processes are necessary mechanisms for the shape of chl distribution in the sub-tropical Pacific. In the second part, the results have been compared with existing datasets of satellite-derived chlorophyll, surface nutrients, estimates of phytoplankton community composition and primary production data. The agreement is reasonable both in terms of the spatial distribution of annual means and seasonal variability in different dynamical oceanographic regions. Results indicate that some of the model biases in chl and surface nutrients distributions can be related to deficiencies in the simulation of physical processes such as advection and mixing. Other discrepancies are attributed to inadequate parameterizations of phytoplankton functional groups. The model has skill in reproducing the overall distribution of large and small phytoplankton but tends to underestimate diatoms in the northern higher latitudes and overestimate nanophytoplankton with respect to picoautotrophs in oligotrophic regions. The performance of the model is discussed in the context of its use in climate studies and an approach for improving the parameterization of functional groups in deterministic models is outlined.

Key words: Global biogeochemical cycles, ocean general circulation model, ecosystem model, OPA, ERSEM, PELAGOS

1 Introduction

The modelling of global ocean biogeochemistry is affected by several uncertainties, partly linked to the poorly-constrained parameterization of biological processes and partly to the proper description of physical variability. Keeping in mind Earth System modelling applications for climate studies, the main aims of marine biogeochemistry models in this context are: 1) to simulate the acclimation of different plankton functional groups to the range of environmental conditions in the current climate ocean, 2) to represent the feedbacks between the pelagic ecosystem and the physical processes and 3) to predict the response of marine ecosystems to climate changes. On the one hand, a proper description of physical processes is the most important prerequisite, because it is well known that gyres, fronts and coastal boundaries are the major discontinuities along which phytoplankton tend to grow and develop due to the co-existence of favorable light and nutrient conditions. Doney et al. (2004) have recently reported that a major fraction of the large model-model spread in the Ocean Carbon Model Intercomparison Project (OCMIP-2) is due to the propagation of known model errors in the representation of physical fi elds in ocean general circulation models (OGCM). On the other hand, current coupled carbon cycle models lack the capability to simulate important biogeochemical processes, mainly because they are based on very simplifi ed assumptions of marine ecosystems' functioning. Recent applications have shown a tendency to increase the number of processes resolved in marine biogeochemistry models (Moore et al., 2002b; Aumont et al., 2003; Gregg et al., 2003; Moore et al., 2004; Manizza et al., 2005; Le Quéré et al., 2005), but many issues are still unresolved (Anderson, 2005). Particularly, the defi nition of the key functional groups and the parameterization of the physiological mechanisms of plankton behavior are important issues that need to be properly considered in biogeochemical model, in order to have reliable predictions on the responses of marine ecosystems and the global carbon cycle to climate changes.

The aim of this paper is to discuss the global ocean implementation of a generic model of pelagic biogeochemistry based on a stoichiometric approach to marine ecosystem modelling and physiological adaptation of organisms to the external environmental conditions. The PELAGOS model (PELAgic biogeochemistry for Global Ocean Simulations) is based on the functional group approach pioneered by the European Regional Seas Ecosystem Model (Baretta et al., 1995; Baretta-Bekker et al., 1997, ERSEM), which has been revisited and extended in a formal background theory described in a companion paper (Vichi et al., 2006, VEA06 hereinafter).

* Corresponding author. Address: INGV, Sezione di Bologna, V. Creti 12, 40128 Bologna. Tel: +39 051 4151 456 Fax: +39 051 4151 499
Email address: vichi@bo.ingv.it (M. Vichi).

Section 2 presents a brief description of the pelagic biogeochemistry model. Section 3 gives the details of the experiment setup, the numerical coupling with the three-dimensional OGCM OPA 8.2 (Madec et al., 1999), the specification of the forcing functions and the derivation of initial conditions. Section 4 is divided in two parts; we first discuss the simulated chlorophyll distribution emphasizing the contribution of the horizontal and vertical physical processes with respect to the local biological rates, taking observed satellite chlorophyll as reference. The second part focuses on the comparison of model results with multivariate datasets. Surface maps of nutrient distributions and phytoplankton community composition are presented for a direct comparison with the World Ocean Atlas (Conkright et al., 2002, WOA01) and preliminary estimates by Alvain et al. (2005). The seasonal variability of chlorophyll, nutrients and phytoplankton composition has been analyzed in selected biogeochemical provinces as defined by Longhurst (1998). A map and list of the Longhurst's provinces is available on the WWW and we refer to the numbering and acronyms defined there (`http://www.mar.dfo-mpo.gc.ca/science/ocean/BedfordBasin/Papers/Longhurst1998/Provinces/EcologicalGeographyOfTheS.htm`). Simulated timeseries have been compared with monthly data from satellite chlorophyll and WOA01, and phytoplankton composition with estimates from the Bermuda Atlantic Time-Series and cruise measurements from Dandonneau et al. (2004). In addition, primary production data from the Joint Global Ocean Flux Studies (JGOFS timeseries and process studies) have been used as benchmarks for validating the simulated production of organic carbon in the different provinces, the major flux affecting the ocean carbon cycle on the annual scale. Section 5, presents a discussion on physical and biological model performances focusing on the role of the different phytoplankton groups and adaptation mechanisms in the simulation of the global carbon cycle.

2 Model description

The PELAGOS model discussed in VEA06 is a biomass-based set of differential equations based on the ERSEM approach to biogeochemical modelling Baretta-Bekker et al. (1995, 1997, and other papers in the two special issues). The model is presented in a generalized mathematical formulation that allows the description of lower trophic levels and major inorganic and organic components of the marine ecosystem from a unified functional perspective. The biogeochemical model is based on the definition of Chemical Functional Families (CFF) as the system state variables. CFFs are further subdivided into living, non-living and inorganic components. Living CFFs are the basis for the definition of Living Functional Groups, the biomass-based functional prototype of the real organisms. Both CFFs and LFGs are theoretical constructs which allow us to relate measurable properties of marine biogeochemistry to the model state variables. They are expressed in terms of several basic components (both elements as C, N, P, Si, O, Fe or molecules as chl), which

are their practical biomass units appropriate for comparison with real observations. As shown in VEA06, the ERSEM model can be easily described in this framework, and moreover such a unified formulation simplifies the extension of the model with additional components. The state variables of PELAGOS representing the pelagic LFGs are three unicellular planktonic autotrophs (picophytoplankton, nanophytoplankton and diatoms), three zooplankton groups (nano-, micro- and meso-) and bacterioplankton. All groups are described with dynamically-varying intracellular quota of the basic constituents, with the addition of chlorophyll in the case of phytoplankton. The other state variables, indicated as chemical functional families in VEA06, are nitrate, ammonium, orthophosphate, silicate, dissolved bioavailable iron, oxygen, carbon dioxide and dissolved and particulate (non-living) organic matter (POM, DOM), for a total of 44 CFF state variables.

PELAGOS is a substantial rewriting of ERSEM and considers some relevant modifications in the trophic structures and biogeochemical cycles which are connected to the global ocean application. One of the major differences with respect to the original ERSEM is the introduction of variable chl:carbon and iron:carbon ratios in phytoplankton, with the addition of a parameterization of the Fe cycle in the open ocean. Iron has significant role in global ocean biogeochemistry, verified by means of direct fertilization experiments (Martin et al., 1994; Boyd et al., 2000) and experimental studies of bioavailability (Coale et al., 1996; Sunda and Huntsman, 1997; Price, 2005). Biogeochemical models have indirectly corroborated this theory because nitrogen- or phosphorus-based models tend to overestimate primary production in all the HNLC regions (Six and Maier-Reimer, 1996; Schmittner et al., 2005) and therefore an additional regulation by iron limitation is required to reproduce the observed low biomass. The implementation of variable internal ratios is valuable for global ocean modelling to adequately represent both the adaptation process, which allows different autotrophs to dominate in a region of the global ocean because of given nutrient and light conditions, and the acclimation mechanism, which permits to overcome short-term variations in the prevailing conditions.

The original ERSEM parameterizations and functional choices were derived from the knowledge of coastal phytoplankton, and considered two major groups, diatoms and non-silicifying autotrophs. The latter group is further divided in size classes, which roughly define their trophic interactions and their physiological rates through allometric considerations. The division between diatoms and non-diatoms is thus functional, while the subclasses in the non-diatom group also have a dimensional criterion. We have not considered large non-edible dinoflagellates (originally in ERSEM) in these climatological experiments because this group is of limited importance in the open ocean. Diazotrophs have been identified as important components of the nitrogen cycle in oligotrophic regions (Karl et al., 2002), and their inclusion will be taken into account in the future for comparison with the current setup.

Most of these groups have been recently revisited by Le Quéré et al. (2005), who

have clearly identified the different functional behavior of the various plankton types at the global scale. Following their ecological and functional classification, PELAGOS considers pico-heterotrophs, pico-autotrophs (comprising both *Prochlorococcus*, *Synechococcus* and eucaryotic picophytoplankton), and mixed nanophytoplankton, in which we include all generic nanoflagellates (haptophytes, without any distinction for calcifiers and their role in the carbonate cycle). As a consequence of the size subdivision in autotrophs, there is a corresponding differentiation in three classes of zooplanktonic predators. The presence of nano- and microzooplankton allows the expression of "microbial loop" and/or "microbial web" trophic dynamics in oligotrophic regions (Legendre and Rassoulzadegan, 1995). Mesozooplankton is represented as one single group, with the clear limitations inherent to treating metazoans in a bulk biomass functional approach.

Let C be a state variable of the model which represents the concentration of either one component of the chosen LFGs (e.g. C-content of diatoms, or a CFF, such as ammoniacal N or P-content in dissolved organic matter. Its dynamics is described by an advection-diffusion-reaction equation (cfr. VEA06 for its derivation):

$$\frac{\partial C}{\partial t} = \underbrace{-\mathbf{u}_H \cdot \nabla_H C + \nabla_H \cdot (A_H \nabla_H C)}_{\text{non-local}} \underbrace{-w\frac{\partial C}{\partial z} + \frac{\partial}{\partial z} A_V \frac{\partial C}{\partial z}}_{\text{local (physical)}} \underbrace{-w_C \frac{\partial C}{\partial z} + \left.\frac{\partial C}{\partial t}\right|_{bio}}_{\text{local (biological)}} \qquad (1)$$

which shows the contributions to the total time-rate of change of C of the non-local (horizontal) advection and diffusion terms, the local (physical) advective and diffusive terms and the local (biological) advective and reaction terms. The distinction made here is the basis for the identification of which physical process contributes to the shaping of observed global chlorophyll distribution that will be presented in Sec. 4.1.

Horizontal and vertical current velocities $\mathbf{u}_H \equiv (u,v)$, w, horizontal and vertical turbulent diffusivity coefficients A_H, A_V, temperature and photosynthetically available surface irradiance are provided by the OGCM OPA 8.2 (Madec et al., 1999) with the global ORCA2 curvilinear grid implementation (Madec and Imbard, 1996). The OGCM has a resolution of 2°of longitude and a variable mesh of 0.5-2° of latitudes from the equator to the poles. The vertical grid has 31 levels with a 10 m step in the top 150 m. The vertical velocity w_C is used to compute the sinking terms of diatoms (as a function of the intracellular nutrient quota, see VEA06) and particulate detritus (constant). The system is fully-coupled as it also provides the biological feedbacks on the short-wave radiative transfer process in the ocean interior.

3 Experiment setup and numerics

The model has been forced with climatological daily surface fluxes from the ERA40 data set averaged over the period 1971-2000 (Uppala, 2001; Simmons, 2001). Daily sea surface temperature (SST) data from the Reynolds data set (Reynolds, 1988) are used to restore the model SST with a relaxation term of 40 W $m^{-2}K^{-1}$ (i.e., a relaxation time scale of approximately 60 d). SST data are also used to compute sea ice cover diagnostically. Wind stress and downward radiation flux are set to zero when the prescribed SST data are below the freezing point, which is computed as a function of the prognostic salinity.

Momentum is diffused with a Laplacian operator and a 2-D spatially-varying kinematic viscosity. The horizontal diffusion of tracers is computed along the isopycnal surfaces as described in Madec et al. (1999) with a constant diffusivity coefficient of 2000 m^2 s^{-1}. Eddy-induced transport is added according to the parameterization by Gent and McWilliams (1990). Vertical eddy diffusion of momentum and tracers is parameterized with a 1.5 turbulence closure model (Blanke and Delecluse, 1993). The background minimum vertical eddy diffusivity is set to 1.2 10^{-5} m^2 s^{-1}. In the case of vertical density instability, diffusivity is enhanced to 100 m^2 s^{-1} in order to parameterize convective adjustments. Temperature and salinity are restored to climatological values below the mixed layer and at latitudes higher than 20^o N and S, with a depth-varying relaxation time of 50 days at the surface and 1 year at the bottom.

The biogeochemical model equations are discretized on the same grid of OPA but the computation of the advection terms in eq. (1) is modified. Advective terms are computed by means of a different numerical scheme, mostly derived from the set of OPA routines for the transport of tracers (Foujols et al., 2000) and by taking into account the work done with OPA 8.1 by Levy et al. (2001) and Estublier and Levy (2000). The need for using positive-definite and monotonic advection schemes strongly affects the computational cost of coupled ecosystem models. The advection of physical variables is instead solved with a second-order centered differencing scheme. This scheme, however, does not satisfy any of the requirements of positiveness and monotonicity, therefore it cannot be used for the transport of biological variables.

Several numerical schemes have been tested for OPA: the Multidimensional Positive Definite Advection Transport Algorithm (Smolarkiewicz, 1984, MPDATA) , another kind of Flux Corrected Transport (FCT) scheme called Total Variation Diminishing (Zalesak, 1979, TVD) and the Monotonic Upstream centered Scheme for Conservation Laws (Hourdin and Armengaud, 1999, MUSCL). Results with a simple biological model (Levy et al., 2001) have shown that TVD and MUSCL perform better than the others. MUSCL has been chosen as the standard advection scheme for this application because of its slightly better computational performances. The

CPU costs of TVD and MUSCL are about three times higher than of the centered scheme. Both TVD and MUSCL lead to similar results in the monthly means, but can differ substantially when comparing instantaneous fields.

The coupling between biological and physical terms is done through a time-splitting integration technique. First the biological reaction term is solved with a simple Euler-forward integration which gives an estimate of the local solution, which is eventually integrated with the standard OPA numerics plus the MUSCL advection. The use of a reversed integration procedure, i.e. physics first and then the reaction term (which would be more appropriate in case of stiff biological terms), did not lead to significant differences at these (large) temporal and spatial scales.

3.1 Initial conditions for biogeochemistry

Physics has been spun up for 30 years with the forcings described above and then the ecosystem model has been coupled using homogeneous initial conditions for all the living functional groups, and with macronutrient distributions from the annual means of the World Ocean Atlas data (Conkright et al., 2002, WOA01). Dissolved iron has been initialized from the sparse data collected by Gregg et al. (2003) by prescribing the profiles shown in Fig. 1 in three zonal bands, the north Atlantic and Pacific, the tropical regions and the Southern Ocean. After 3 years of simulation most of the regions have reached a repeating seasonal cycle in the 100 m average of all the variables and the results are shown here for the 4th simulation year.

3.2 Surface boundary conditions for biogeochemistry

The deposition of mineral dust is an important boundary conditions generally taken from numerical models (Tegen and Fung, 1994; Gao et al., 2003). The solubility of iron in aerosols is one of the major uncertain factors that hamper a consistent inclusion of these deposition fluxes. Solubility in sea water has been observed to span several orders of magnitude in laboratory experiments, with values ranging from 1% to 50%. Continental margins are also a possible large source of iron to the surface open ocean (Johnson et al., 1999). Another important source is the regenerated iron flux at the sediment-water interface, which has recently been estimated to be as relevant as the atmospheric inputs (Elrod et al., 2004). These sources are now being partially parameterized in global models (Moore et al., 2004), although both coastal processes and resuspension dynamics occur at time-scales that are currently not resolved in global OGCMs and benthic remineralization fluxes are not taken into account.

The only external forcing function for our biogeochemical model is the monthly atmospheric iron dust deposition that is taken from climatological model data by

Tegen and Fung (1994). The dissolution fraction of iron dust is set to 1%, the same as used in the simulations of Aumont et al. (2003) and Gregg et al. (2003). As pointed out by Moore et al. (2004, 2002a), there are many uncertainties related to the major processes comprising the iron cycle (dissolution, bioavailability and scavenging), and they have shown that variations in atmospheric iron dissolution have substantial impacts on the large scale ocean production. Preliminary sensitivity experiments with our model indicate a generalized increase in primary production of 15-20% when the dissolution fraction is raised to 5%, confirming the need for further investigation of the dissolution mechanisms and to decrease the uncertainties in this external forcing function.

No-flux surface boundary conditions are prescribed for all the biogeochemical state variables other than iron.

4 Results

4.1 Physical-biological processes and chlorophyll distribution

The global distribution of chl observed from space shows large scale patterns that can generally be explained by distinct physical regimes. This is the basis of the concept of biogeochemical provinces (Longhurst, 1998), and most of these large scale signals can also be captured by much simpler NPZD models that take into account the light and nutrient dependence of phytoplankton production and the physics of the mixed layer (e.g. Six and Maier-Reimer, 1996). More complex models such as PELAGOS provide additional information on the biogeochemistry and plankton distribution, but since ocean color sensors are the only instruments that provide a proxy for the global near-surface distribution of primary producers, also complex models of necessity have to be validated against this bulk property.

In this section we investigate the contribution of physical and biological terms in determining the simulated chl distribution, comparing it with the chl estimates derived from the ocean color SeaWiFS sensors (L3 Standard Mapped Images) averaged over the period 1998-2003. In the following analyses shelf areas, where physical processes are insufficiently captured by the coarse OGCM, have been masked, as well as points where satellite data are not available. Satellite chlorophyll has been derived from model chl as

$$chl_{sat} = \frac{\int_0^{Z^*_{od}} chl(z)\, e^{-\lambda(chl)z} dz}{\int_0^{Z^*_{od}} e^{-\lambda(chl)z} dz} \tag{2}$$

where $Z^*_{od} = \varepsilon Z_{od}$ is the optical depth Z_{od} where downwelling irradiance is attenuated by a factor e^{-1}, scaled by a constant correction factor $\varepsilon = 1.5$ that takes into

account the effect of the vertical discretization on the chl distribution (ε should tend to 1 as the vertical resolution increases). The attenuation coefficient λ is computed as the sum of the attenuation by the phytoplankton chl plus the optical background extinction and the effect of attenuation by particulate organic matter (see VEA06). The optical depth is about 30 m in the subtropical oligotrophic regions and is limited to the first layer (10 m) at high latitudes and in the equatorial Pacific.

Three numerical experiments have been run to separate the physical and biological terms, with the configurations described in Table 1. It is important to point out that these configurations do not affect the physics, but only the way in which the physical terms are combined with the biological reaction term in eq. (1). The biological vertical sinking is always applied because it is considered to be a local biological term. Configuration C3 thus represents a collection of one-dimensional water-column models, the typical setup used to test the parameterizations of coupled biogeochemical-physical models.

Panel a in Fig. 2 shows the annual mean distribution derived from SeaWiFS satellite data characterized by typical minima in the subtropical gyres and maxima in tropical upwelling regions. The full model in C1 configuration (panel b) captures the major features but underestimates the chl values particularly in the North Atlantic and north-eastern Pacific, and overestimates in the stratified subtropical gyres. The coarse resolution of the OGCM is mostly responsible for the partial absence of many coastal upwelling areas, such as the Moroccan and Peruvian regions, as well as other typically coastal features affected by land-derived nutrient inputs.

A comparison with experiments C2 and C3 highlights the effects of horizontal advection and diffusion (A-D) terms (C2) and vertical advection (C3) on the chl concentration in the gyres. A-D are necessary mechanisms for the shaping of chl distribution in the equatorial Pacific but they lead to a general overestimation of tropical surface values very likely due to the fact that the currents are not properly represented in the OGCM. This is particularly evident in the large chl band covering the North Pacific Subtropical Gyre region (Longhurst, 1998, NPSG), which is associated with the transport of upwelled equatorial nutrients and biomass. This feature is persistent throughout the year and masks the oligotrophic characteristics of the NPSG province. The convergence in the subtropical gyre is due to a likely overestimation of the northward component of the gyral velocity in the OGCM (not shown).

Nevertheless, the C1 simulation is able to capture the proper westward extension of the pacific equatorial chl maximum, while it is clearly overestimated in C2 and obviously absent in C3 due to the suppression of any local upwelling process. The latitudinal spreading in C1 is slightly overestimated which is probably due to the spatial resolution that is still too coarse.

It is interesting to note that the Ekman pumping in the middle of all the subtropical

gyres and the downwelling of cold waters from 5 to 15°S both counteract the effect of nutrient replenishment due to turbulent mixing, leading to lower chl values in C2 with respect to C3. In the Southern Pacific Subtropical Gyre region (SPSG) the advection of nutrients from the equator in the C1 simulation tends to restore conditions similar to C3. In the southern Indian Ocean, instead, A-D terms lead to a clear overestimation of chl values and the oligotrophic structure of the gyre is well defined only in run C2.

In the northern Indian Ocean, model runs in C1 and C2 configurations show only a small bloom in the Arabian Sea related to the monsoon regime, while the maximum covers the whole northern part of the Indian basin in the satellite data. In the whole northern Indian Ocean the model produces a Deep Chl Maximum (DCM) in coincidence with the location of the nutricline/thermocline at about 100 m. However, WOA01 data suggest that the tilting of the nutricline is much more pronounced, probably due to an intensification of the upward flux of nutrients from the deep reservoirs which is not properly resolved by the model.

The amplitude and distribution of C1 chl (Fig, 2b) agree well with the satellite observations in the Southern Ocean, especially because of the introduction of Fe limitation in the phytoplankton equations. The persistence of patches of chl associated with the movement of the South Subtropical Convergence zone in the austral Indian Ocean and in the southern Atlantic and the retroflection of the East Australia Current (Longhurst, 1998) are correctly reproduced, but there is an overestimation of chl in the regions connecting these patches. This large band of 0.2-0.3 mg m^{-3} is mostly due to vertical mixing processes as indicated by the results of run C3. The simulated mixed layer in the Sub-Antarctic province (SANT) during the austral spring (Fig. 3a) is up to 70 m shallower than the climatology collected by de Boyer Montégut et al. (2004). The shallower mixed layer favors the phytoplankton acclimation to low-light conditions and an early start of the bloom (see also Sec. 4.5). The spatial structure of the stratified waters is also quite homogeneous, while it has been suggested that the path of the Antarctic Circumpolar Current (ACC) is seeded with spots where strong diapycnal mixing occurs (Garabato et al., 2004). Such hot spots are visible in the simulated chl field of run C2, where the removal of non-local terms makes the contribution of the vertical eddy-induced upwelling more evident. Another interesting feature related to local physical processes is the presence of high chl values along the Antarctic coastline which are clearly visible in the C2 run, and to a lesser extent also in C3. The inclusion of A-D terms leads to a dissipation of the coastal maxima and to a generalized diffusion of chl in the whole ACC.

In the north Atlantic, the model underestimates the mean annual observed value in all simulations, particularly in the eastern part in correspondence with the branching of the Gulf Stream. Only run C2 has slightly higher chl values especially in the Norwegian and Greenland Seas, but in general the discrepancy cannot be ascribed to one single physical term. Model results are probably hampered by the poor simu-

lation of the Gulf Stream path at this coarse resolution, but also by a too strong light limitation during the late autumn-winter period that leads to low biomass and biases the annual mean. Indeed, the intensity and distribution of the spring bloom (AMJ, Fig. 4) is rather well captured in the whole north Atlantic. The major discrepancy is the absence of high chl in the northern flank of the Azores current departing from the branching of the Gulf Stream.

Low biomass are visible in the northern Labrador basin and in the Denmark Strait, but also in the Southern Hemisphere below 50°S. We believe that the low biomass values in these regions are due to light limitation and not to model resolution as is the case in other coastal areas. The same northern regions reach higher values of chl if we take the early summer mean (cfr. Fig. 7, left panels), when the pattern of the bloom is more similar to the observations.

4.2 Nutrient distributions

The analyses presented in this section and in the following ones will focus only on model results from the C1 configuration, the experiment that contains the full physics. This section will show a comparison with global nutrient distributions, which are the most significant bulk properties of ocean biogeochemistry for which statistical global analyses are available (Conkright et al., 2002).

Model-derived annual means of surface nutrient concentrations are directly compared with the WOA01 data in Fig. 5. The values and extension of the north Atlantic maxima are matched for all nutrients despite the bias in the chl distribution (Fig. 2). The major discrepancy at these latitudes is in the north-east Pacific sub-Arctic region, where all simulated nutrient concentrations are too low with respect to the observations, and where also chl is underestimated (Fig. 2). This discrepancy can be explained by a reduced replenishment of nutrients during the well-mixed winter period. Indeed, the mixed layer depth simulated by the model in this region (Fig. 3b) is much shallower during winter than the de Boyer Montégut et al. (2004) climatology. This implies that nutrient replenishment is much reduced in the simulation. In addition, Fe limitation may further contribute to low chl values. The eastern sub-arctic Pacific region is a well-known HNLC area (Martin and Fitzwater, 1988) where iron availability is thought to play a substantial role. Indeed, the simulated surface distribution of mean dissolved iron (Fig. 6) gives values that are typical of HNLC regions (Martin et al., 1991; Coale et al., 1996). An experiment where iron dust solubility was increased from 1% to 5% showed an enhancement of chl concentration which matched the observations without any increase in the simulated surface iron concentration. This supports the idea that in the north-east Pacific additional iron sources are necessary to reproduce observed values and coastal sources are likely to be a relevant portion of this total supply.

The simulation of nutrient features in the subtropical and intertropical regions of the world ocean is problematic as also shown by the results of other modelling efforts (Moore et al., 2004; Schmittner et al., 2005). The annual mean nitrate distribution predicted by PELAGOS nevertheless is adequate, especially in reproducing the magnitude of the eastern equatorial upwelling plume in the Pacific. On the other hand, the latitudinal extension in the western part is overestimated for both phosphate and silicate, most likely as a result of an imperfect simulation of the subtropical gyre circulation in the OGCM (cfr. Sec. 4.1). Nutrients, which cannot be consumed in the equatorial region because of iron limitation, are eventually available for phytoplankton growth inside the gyre where iron is present due to atmospheric deposition and diffusion (cfr. Fig. 6).

The tropical Atlantic is affected by a strong simulated depletion of phosphate and silicate which is only partly observed in the data. The simulated minimum of phosphate in the northern tropical Atlantic (NATR) is a feature also found in the results of Moore et al. (2004) and explained as the consequence of excessive nitrogen fixation rates early in the simulation. However, the same conditions are obtained here in the absence of nitrogen fixation, suggesting that phosphate depletion is probably due to the lack of land-derived nutrient inflows from the Amazon and Orinoco rivers that have been shown to extend far into the North Atlantic gyre (Conkright et al., 2000). The same considerations can also be applied to silicate, another nutrient which is strongly determined by river loads.

Too low concentrations of surface nutrients are simulated in the northern Indian Ocean (Arabian Sea and Bay of Bengal), a well-known upwelling region associated with the monsoon regime (Banse, 1987). As discussed above, this discrepancy is probably due to the limited capability of coarse GCMs to provide the proper upwelling dynamics in shelf regions and this deficiency affects the chlorophyll concentrations as well (see Sec. 4.1). It is also important to bear in mind that additional phosphate and other nutrients are released by the Indo, Gange and Brahmaputra rivers as a result of increased flow during the monsoon rain season (Conkright et al., 2000) and therefore the simulation would very likely benefit from the inclusion of land-derived nutrient inputs.

There is still not enough information to validate the surface distribution of Fe (Fig. 6b), which in the model is mostly determined by the deposition patterns of atmospheric iron dust (Tegen and Fung, 1994, see Fig. 6a). The lowest concentrations in the model are found in the SPSG region and in the western tropical Pacific because these areas are not affected by any land-derived dust flux. In the Pacific Equatorial Divergence (PEQD) iron is provided by upwelling of iron-rich deeper waters (cfr. Fig. 1). The subsurface increase in iron concentration in the PEQD has been suggested to be enhanced by eastward advection from iron sources in the western Pacific shelves with the Equatorial Under Current (Mackey et al., 2002). The simulated iron surface concentration in the upwelling region is generally below 0.1 μmol m^{-3} on average, as observed during the JGOFS campaigns (Coale et al.,

1996; Gordon et al., 1997).

Similar concentrations, in spite of the total absence of surface deposition, are found in the Southern Ocean as a result of upwelling processes as well. We report here that the use of a Droop-like quota model in the phytoplankton iron parameterization leads to higher ambient concentrations with respect to a Michaelis-Menten formulation. Surface biomass is therefore higher in the simulation results shown here, while the use of a Michaelis-Menten parameterization would require an increase of the dissolution rate of iron dust to obtain comparable concentrations.

4.3 Spatial distribution of phytoplankton groups

The differentiation of "Phytoplankton" into functional groups of primary producers is needed to track the fate of biogenic organic matter in climate models, because potential carbon sequestration is a function of the size and quality of the organic products. Availability of phytoplankton assemblage data is unfortunately limited for global scale validation. In following sections we will validate the model in those biogeochemical provinces where direct phytoplankton composition data can be derived from High-Performance Liquid Chromatography (HPLC) pigment measurements according to the classification of Jeffrey (1997) and Dandonneau et al. (2004). In this section we present the simulated monthly distributions of phytoplankton groups and corresponding total chl (Fig. 7), which may be compared with the estimates derived by empirical regression analyses of coincident in situ measurements and ocean color data as proposed by Alvain et al. (2005, their Fig. 6).

Model results and satellite data have to be compared with some caveats, as they have been derived with different criteria which depend on the specific methodology. Values of total chl lower than 0.05 have been masked and relative chl concentrations higher than 0.33 for each group have been marked with a colored pixel. The choice of the threshold is crucial in determining the dominance of one group with respect to others, and there are cases, especially in oligotrophic regions, where pico- and nanophytoplankton are equally abundant. It is thus not possible to assign an absolute dominance flag and these cases will be further discussed in the next sections. Another note of caution is related to the different time scales considered. Alvain et al. (2005) data are derived from year 2001, while the model results represent a climatological situation without any interannual variability.

The model predicts that diatoms are always dominant in the north Pacific and in the ACC, although winter total chl is rather low and therefore this standing stock is the background winter concentration and not an indication of a continuous production phase. The simulated diatom bloom in the Southern Ocean, detected by a combination of high chl and diatom dominance, is larger in October in the ACC, while

the data by Alvain et al. (2005) give indications of a later bloom in January. The simulated diatom behavior is consistent with the results shown in Sec. 4.5, hinting at a temporal mismatch in the stratification regime. The North Atlantic is characterized by a double bloom of diatoms in the model (a spring bloom in the Gulf Stream drift region and an autumn bloom at higher latitudes) with a shift towards smaller species during summer.

The model has a poor representation of chl in the major coastal upwelling regions (e.g. Morocco and Arabian Sea, cfr. Sec. 4.1), but clearly shows that the local simulated production is mostly due to diatoms, and the seasonal cycle is particularly well reproduced in the Arabian Sea during the monsoon periods. Alvain et al. (2005) data never show diatoms dominating in the northern Indian Ocean, but this region has the highest fraction of unidentified pixels in their analysis.

Picophytoplankton mostly dominates in the equatorial band and it is as abundant as nanophytoplankton in the subtropical gyres (cfr. also section below and Fig. 9). The largest discrepancy in the simulation of picoautotrophs is the January bloom in the Southern Ocean, which is not found in the satellite estimates, although several unidentified pixels are present. A similar discrepancy is also found in June in the northern North Atlantic. Picophytoplankton dominate the phytoplankton assemblage during August in the sub-arctic regions of the Pacific and Atlantic oceans, a feature also visible in the data presented by Alvain et al. (2005). The model thus predicts a clear shifting towards smaller groups after the depletion of surface nutrients in these regions.

In the model nanophytoplankton is the most widespread group in the temperate regions of the southern hemisphere. In the northern hemisphere they are instead characterized by an early summer bloom in the northern North Atlantic and an autumn one in the north-eastern Pacific. The subtropical gyres in the southern hemisphere are also dominated by this group for most of the year, which agrees well with the maps of Alvain et al. (2005), particularly in matching the absence of haptophyte blooms in the Southern Ocean polar front.

4.4 Seasonal cycles: Atlantic Ocean

The seasonal analysis is presented in this section for 3 of the Atlantic provinces defined by Longhurst (1998): the North Atlantic Drift Region (NADR), the North Atlantic Sub-Tropical Gyral province (western limb, NASW) and the South Atlantic Gyral province (SATL). Seasonal cycles will be compared with bulk properties (chl from SeaWiFS and CZCS) and also with phytoplankton group composition derived from HPLC-analyzed pigments. Data from the GEP&CO cruises (1999-2001) elaborated by Dandonneau et al. (2004) have been used in the NADR province, while the long-term pigment observations at the JGOFS Bermuda Atlantic Time Series

study site (Michaels and Knap, 1996, BATS) have been used as representative of the NASW province.

The left panels in Fig. 8 present the time evolution of the phytoplankton characteristics (chl and assemblage composition), and the right panels of the same figure show the corresponding simulated seasonal cycles of phosphate, nitrate, silicate in the same province. The NADR region (upper panels) typically shows deep winter mixing with a spring bloom starting in late April and May and a fast depletion of nutrients during summertime (Longhurst, 1998). Simulated chl concentration is extremely low in the starting phase of the bloom, and therefore the simulated diatom dominance is not representative. GEP&CO data (Dandonneau et al., 2004), show that the spring period is equally represented by diatoms and nanophytoplankton while the model has a clear predominance of diatoms. The post-bloom conditions are in much better agreement with the GEP&CO data, with a shift towards flagellates, but the summer chl concentration is too low probably because diatoms are less represented. The simulated nutrient evolution is within the observed ranges, apart from phosphate which is brought to lower levels during the bloom in May. This is consistent with a shoaling of the mixed layer significantly faster than the observed one (see Fig. 3c) which reduces the diffusion of nutrients from the deeper layers. The lower silicate values observed in the data with respect to the simulation indicate that in reality diatoms persist during the whole year as shown in GEP&CO data.

The North Atlantic Subtropical Western gyre province (NASW, middle panels) is characterized by winter mixing of variable duration which brings nutrients in the euphotic zone and a short chlorophyll peak from February to April (Longhurst, 1998). These features are well captured by the model in the corresponding bulk chl evolution. The winter nutrient replenishment is slightly visible in the WOA01 (Fig. 8b) while it is overestimated in the model (particularly in nitrate), leading to a higher bloom peak which is nevertheless within the observed ranges. The model correctly reproduces the dominance of nanoflagellates over the other groups as observed at BATS, but overestimates the contribution of diatoms (not the seasonal variability, which is instead well represented with a slight increase in April and another one in Autumn).

It has been shown in Sec. 4.2 that the North Atlantic Tropical Gyral province (NATR) is affected by a strong depletion of nutrients throughout the year. On the other hand, the South Atlantic Gyral Province (SATL) is very well simulated both in terms of the magnitude and seasonal variability of nutrients and chl (Fig. 8, bottom panels (d)). This is probably due to the southern boundary defined by the ACC convergence and the persistent influence of the trade winds that impose a somewhat "simpler" seasonal variation on this gyral region than its North Atlantic equivalent. SeaWiFS chl data show a bimodal time-evolution, which is present neither in the CZCS data nor in the model. The model predicts a small increase in surface chl in austral winter, which is caused by the subduction of nutrient rich waters from

the ACC that induces a bloom in the southern part of the gyre. As pointed out by Longhurst (1998), this is one of the least studied oceanographic regions and more large-scale surveys are needed to better understand its main characteristics.

4.5 Seasonal cycles: Pacific and Southern Oceans

In the Pacific we have chosen the southern tropical and subtropical gyre (SPSG), the Pacific Equatorial Divergence (PEQD) and, as representative of the Southern Ocean, the Sub-ANTarctic polar front province (SANT, Fig. 9).

In the Southern Pacific Subtropical Gyre (Longhurst, 1998, SPSG) there is an austral winter increase in chl which is well captured in the simulation and is linked to a weak deepening of the mixed layer. It is interesting to note that the largest spatial variability in SeaWiFS data is found during the austral summer period and is mostly due to the influence of the Peru-Chile current coastal region which was included in our spatial average. According to GeP&CO observations (Dandonneau et al., 2004), the SPSG is dominated by picophytoplankton which is always more than 50% of the assemblage (mostly *Prochlorococcus*), while the model predicts a persistence of nanoflagellates. The winter mixing does not lead to an increase in nutrient concentrations (left panel in Fig. 9a) indicating that nutrients are readily used by phytoplankton because of the permanent oligotrophic conditions. The largest discrepancy is found in silicate, which is always overestimated due to an expansion of the nutrient-replete polar front across the southern border of the gyre (cfr. Fig. 5).

The Pacific Equatorial Divergence (PEQD) has been extensively studied in past years as a typical example of HNLC area (Martin et al., 1994; Coale et al., 1996). This province is characterized by extremely low seasonality in chlorophyll biomass, a feature remarkably well captured by the model (Fig. 9b). The phytoplankton community mostly comprises the nano and pico size fraction as also observed in the GEP&CO data (Dandonneau et al., 2004), although the model still predicts a slight dominance of nanoflagellates. All nutrients are generally overestimated especially in the first part of the year, and in the case of silicate the bias is larger. The reason of this discrepancy is still unknown but it might be related to changes in the silica requirements of diatoms under iron-deficient conditions as suggested by Takeda (1998), a feature not in the model.

The average annual distribution of chl in the Southern Ocean is well captured by the model (Fig. 2), and also the seasonal variability is broadly consistent with the observed ranges in the sub-Antarctic region (SANT, Fig. 9c). The austral summer bloom, however, is significantly overestimated and mostly consists of picophytoplankton (cfr. 4.3). This can be explained by a sudden onset of growth-favorable stratified conditions simulated by the OGCM in this province (Fig. 3a). The pi-

cophytoplankton dominance is in contrast with the prevalence of diatoms in the frontal zones of the Southern Ocean (Laubscher et al., 1993; Semeneh et al., 1998), although regions with high picophytoplankton abundance have been reported in the Atlantic sector (Froneman et al., 2001) and Alvain et al. (2005) estimates do show the dominance of *Prochlorococcus* in some areas. The phytoplankton composition in February is much more in agreement with the observed shift towards nanophytoplankton dominance in late austral summer (Laubscher et al., 1993).

The excess of silicate is particularly evident in this province, where modeled concentration is about three times higher than the WOA01 mean, despite the correct simulation of the other macronutrients (Fig. 9c). Data from the JGOFS timeseries at the Kerguelen plateau (Jeandel et al., 1998, KERFIX) indicate an austral spring phytoplankton bloom of about 1 mg chl m^{-3} and a signifi cant drawdown of surface silicate in the boreal summer that is also visible in the WOA01 and SeaWiFS data. This feature was simulated in a one-dimensional model at KERFIX only by applying substantially increased Si:N uptake ratios of 3-5 mol Si (mol N)$^{-1}$ (Pondaven et al., 2000). The value used in our model (0.8 mol Si (mol N)$^{-1}$) is more suitable for sustaining diatom growth in mid-latitude North Atlantic regions such as NADR, where the winter concentration of silicate is 3 mmol m^{-3} (Fig. 8a) and therefore the utilization of silicate by diatoms in our model is much reduced in this region with respect to the other nutrients.

4.6 Primary production

Figure 10 presents an overview of the modeled gross primary production (PP) compared with the data collected at the various JGOFS study sites (see Ducklow, 2003, for an overview). This comparison is made to show that the model broadly captures production rates characteristic of different biogeochemical provinces, which is a prerequisite for modelling the geographical diversity of the biological pump in a climate study context. Since several sites have limited number of observations we have chosen to compare the surface values because these are almost always available in the data sets. Model and data have been compared for the same location and period of the year, but clearly process studies such as the Equatorial Pacifi c (EQPAC) cruises in 1992 are less representative of a climatological situation than the continuous timeseries collected at the Hawaii Ocean Timeseries (HOT) or at the Bermuda station (BATS).

EQPAC data revealed extremely high PP rates that the model is not able to reproduce in a climatological simulation (Fig. 10). The EQPAC measurements are also much higher than the values reported in Longhurst (1998), and our simulated values are closer to the fi eld observations than to Longhurst's estimate. BATS and HOT mean PPs are comparable in the model as they are in the data, which is striking when considering the different physical regimes (Ducklow, 2003). The model PP

might be biased to higher values by the problems of transport in the gyres discussed in Sec. 4.1, therefore an improvement in the physics representation is expected to improve also the agreement with the JGOFS observations.

The highest PP mean values are found in the Arabian Sea and in the Antarctic Polar Front Zone (APFZ) during the austral summer. These maxima are well captured in model results, indicating that the carbon fixation process is sufficiently well parameterized to reproduce the phytoplankton features at these contrasting sites. The fact that gross PP is comparable with data in the northern Indian Ocean but not the biomass (Fig. 2) has to be ascribed to the low surface nutrient concentrations simulated by the model. Since carbon and nutrient dynamics are decoupled in the model (cfr. VEA06), gross production continues despite the lack of nutrients, but formation of biomass (net production) is low.

The APFZ site attains the highest value among the JGOFS sites in the model. The polar front can support high PP during summer because optimal conditions of stratification and iron availability favor phytoplankton growth. The autumn value is instead underestimated, hinting at the problems related to chl turnover discussed in Sec. 4.1. The Ross Sea mean PP is also underestimated, although within the observed range of variability which is rather high.

The seasonal cycle of PP is shown in Fig. 11 for the BATS and HOT timeseries, where 10 years of data allow us to reconstruct a meaningful seasonal climatology. The two sites are representative of the northern subtropical gyres but BATS is more affected by the seasonal variability associated with the Gulf Stream whereas HOT is a typical oligotrophic site with little variability. The difference between the regions is well simulated by the model, despite the discrepancy in the spring maximum at BATS. The model in fact mirrors the observed average value of chl in the whole NASW region (cfr. 8) with a maximum of biomass production in April. BATS data are earlier by about two months, indicating the dominance of local physical processes which are not captured by the coarse OGCM.

5 Discussion

The results presented in this study demonstrate the implementation of a coupled multi-component model of general circulation and pelagic biogeochemistry , as a preliminary and necessary step towards Earth System modelling applications. The model applied here at the global scale inherited the biogeochemical approach from ERSEM, which was extensively validated at the regional scale, but mostly in temperate regions. If it is assumed that primitive functionalities of plankton behavior do exist in the ocean, then a global implementation of a generalized biogeochemistry model is a suitable method to validate the parameterizations. However, although having a unified modelling approach that can be applied to regional and large scale

processes is a clear advantage, there is a lack of studies that investigate the behavior of such parameterizations at different spatial and temporal scales, and how to include subgrid-scale biological dynamics into coarse resolution models (e.g. Fennel and Neumann, 1996). A first prerequisite for this kind of studies is a unified mathematical formalism to describe the biogeochemical interactions, as the one suggested in VEA06, in order to achieve a general consensus on the form of biomass-based biogeochemistry model and eventually proceed to more extended unification of the different types of marine ecosystem models (Fennel and Osborn, 2005).

The tendency of state-of-the-art biogeochemistry models embedded into OGCM is to increase the number of LFGs (or Plankton Functional Types, PFT, if referring to pelagic groups only) in order to capture the complexity and diverse features of the plankton environment (Moore et al., 2002b; Gregg et al., 2003; Moore et al., 2004; Le Quéré et al., 2005). This approach is prone to criticism, because the ecology of plankton groups is poorly understood and the direct incorporation of complex models into global OGCM without thorough testing at the regional scale might lead to unpredictable behavior (Anderson, 2005). The discrepancies with observations seen in the results of the existing coupled physical-biological models of the global ocean are in fact partly due to inadequate parameterization of biological processes but also to an insufficient description of the physical features in the coarse OGCMs that are used for this type of applications. The uncertainties on both processes are one of the reasons for the skepticism about the inclusion of more complex biogeochemical models into climate studies (Sarmiento et al., 2004).

In the first part of this work we have investigated part of these uncertainties by studying the relative contribution of dfferent physical and biological terms to the surface distribution of phytoplankton. Our analysis focused on bulk chl because of the satellite data availability, but can also be repeated for each single phytoplankton group to identify the specific response to different physical regimes. The method we applied was to sequentially neglect the non-local horizontal transport terms and the vertical local terms in the biogeochemical equations, and to study the numerical solution of the resulting simplified equations. On the one hand this approach allowed us to identify regions of the world ocean where observed chl distribution can be largely explained by local mixing and upwelling processes. On the other hand it allowed us to trace some of the model biases in chl and surface nutrients to deficiencies in the simulation of the OGCM transport processes that do not show up in the distribution of other surface physical properties (e.g. temperature and salinity), since these are either constrained by air-sea fluxes or restored to observations. The unrealistic simulation of the seasonal cycle of mixed layer depths in several regions (cfr. Fig. 3) is also clearly a factor that contributes to these biases and needs to be improved in global OGCM.

This paper clearly shows that the simulated annual average of chl distribution is to a large extent determined by vertical hydrodynamical processes which are local by definition. Mixing controls simulated chl at high latitudes and vertical advection

is the major mechanism responsible for the equatorial intensification. Horizontal transport is necessary to obtain the observed shape of the southern Pacific equatorial divergence but tends to overestimate the chl in the gyres because of the excessive transport of nutrients from the nutrient-replete regions of the equator and the sub-Antarctic polar front. This can also be due to biological factors such as a reduced nutrient utilization in the HNLC regions which might be caused by higher nutrient requirements under iron-limited conditions (e.g. Takeda, 1998) .

Model results show that coastal upwelling processes, where a substantial part of the global primary production occurs, are only weakly captured at this coarse spatial resolution. The Arabian Sea chl maxima are largely underestimated in terms of biomass and the other west Africa upwelling regions are weakly represented. Insufficient winter mixing and lack of land-derived iron inputs are instead likely to be the cause of the underestimation of nutrients and chl in the eastern sub-Arctic Pacific. As pointed out by Doney et al. (2004), some deficiencies of the physical model are reflected in the results of the biogeochemistry and especially coastal boundary processes (with the addition of land-derived nutrient inputs from the shelves) need to be refined in order to provide the appropriate physical and chemical conditions suitable for plankton development.

The above considerations apply to bulk properties of the phytoplankton which are mostly controlled by the interactions between large scale physical features and the controls imposed by light and nutrient availability. These features can also be captured by simpler NPZD-like models but models like PELAGOS can provide additional information on the behavior of the various functional groups. This application in fact revealed some discrepancies in the analyzed bulk properties that are not directly due to the physical parameterization but can be ascribed to inadequate parameterizations of a specific functional group, inferred by a direct comparison of model results with data on phytoplankton composition. It is therefore important that such data are collected on a routine basis (e.g. Dandonneau et al., 2004, and the JGOFS time-series) and that global compilations of pigment data are made available for direct comparisons with models.

The model predicts winter chl concentrations lower than observed in the northern high latitudes, despite the proper simulation of nutrient availability (cfr. Figs. 7 and 5). This results in an overall underestimation of the annual average of biomass particularly in the North Atlantic (Fig. 2). The analyses of the different phytoplankton groups done in Sec. 4.3 and following sections give indications that diatoms are misrepresented in these regions. An improvement of results can be obtained either by increasing the maximum light utilization coefficient in diatoms or by modifying the form of the chl equation to enhance the decoupling between the synthesis of chlorophyll and turnover. The overestimation of the mixed layer depth in boreal winter in the same region (cfr. Fig. 3c) is also a possible explanation of the diatom underestimation, which can be due to excessive mixing under surface low-light conditions. The summer underestimation in the NADR is probably due to the sim-

plified parameterization of sinking rates. Diatom sinking velocity increases under nutrient limitation (nitrogen in this case, cfr. VEA06), and the diatom maximum is located at around 60 m in this region, well below the optical depth used in the model to compute the chl value. Further investigations, also performed with the aid of one-dimensional models, are thus needed to better understand and quantify the acclimation processes of diatom survival at extremely low nutrient or light conditions.

The oligotrophic subtropical gyres are instead dominated by smaller phytoplankton as found in data by Dandonneau et al. (2004) and proxies of distribution maps by Alvain et al. (2005), but the model generally tends to show a prevalence of nanoflagellates over picophytoplankton. In the original ERSEM formulation, affinity constants for nutrients were set equal for all phytoplankton groups because land-derived inputs dominated the availability of nutrients, and also benthic-pelagic exchanges contributed additional nutrients. Therefore, extremely low nutrient concentrations in coastal regions occur only during the summer stratified period and not throughout the year as in the subtropical oligotrophic gyres. It is likely that affinity constants need to be adjusted for global ocean applications, making picophytoplankton more adapted to survival at very low ambient concentrations of inorganic nutrients with a consequent increase of their biomass particularly in the SPSG region.

Other substantial discrepancies in the phytoplankton distribution predicted by the model are the persistence of diatoms in the antarctic polar front and the large summer bloom of picophytoplankton off the Antarctic coast. This latter is the result of the combination of several independent factors: the absence of a temperature control (mostly for *Prochlorococcus*, Partensky et al., 1999), the low Fe requirements (Timmermans et al., 2005), the persistent spring-summer stratification (cfr. Fig. 3a) and the lack of nanoplanktonic grazers that could not survive the winter conditions and cannot therefore graze down the bloom. Grazing pressure is very low during early summer, mostly because phytoplankton concentrations are low. Zooplankton control during the bloom development and during overwintering clearly plays an important role in controlling phytoplankton biomass, but the global impact of these processes have not been thoroughly analyzed in the model yet. Diatoms indeed can survive the whole year in the front although at low concentrations (Fig. 7). The subduction of colder nutrient-rich Antarctic waters creates a favourable environment for the maintenance of the standing stock, particularly because iron is provided as well (Fig. 6b) through deep mixing processes. It is likely that these conditions are more intermittent in reality (Garabato et al., 2004) leading to a co-limitation of iron and light availabity

The rates of primary production predicted by the model are obtained from a climatological simulation and since primary production is a fast and local process, such a coarse resolution model can only aim at capturing the observed magnitude. Data are collected only at selected sites and during time-limited process studies

(Ducklow, 2003), or alternatively, proxy information may be derived from satellite chl data (Behrenfeld and Falkowski, 1997). We preferred to use the independent JGOFS data to validate the model and the intrinsic limitations of a direct comparison have been partially avoided by considering the same period of the year when data have been collected. The analysis of the two long time-series at BATS and HOT shows that the simulated seasonal variability is directly linked to the representation of physical processes, and therefore some bias can be observed. Nevertheless, the comparison shown in Sec. 4.6 indicates that the overall gross production of organic carbon is reasonably simulated in different areas of the world ocean, which increases our confi dence in the biological processes affecting the uptake of aquatic CO_2 at the temporal and spatial scales of climate dynamics. A direct validation with observed CO_2 fluxes is also needed in the future to directly assess the effects on the atmospheric concentration.

6 Final remarks

The overarching question that has been posed throughout this work is how to reconcile the complex behavior of plankton communities, which can only be directly measured in small regions of the ocean where mesoscale physical features play an important role, and the representation of these communities in climate-oriented OGCM, where those small scales cannot be resolved for obvious computational reasons. Our answer follows two complementary approaches: on the one hand we want to clearly defi ne the formulations employed to identify the basic model assumptions (see Vichi et al., 2006), and on the other hand we want to check the genericity of the model by applying it both in coastal/regional models (where validation data are more abundant) and in the global ocean.

ERSEM and its descendants have been thoroughly analyzed in regional coupled models, but this is not a guarantee of success in the global ocean. Given the limits of the coarse OGCM, the results shown in this paper are indicative of a reasonable behavior of the biogeochemistry model, both from the point of view of bulk properties and from the global distribution of the selected phytoplankton groups. Nevertheless, there are no outstanding indications, by just looking at the surface fi elds of chl and nutrients, that a detailed physiological model is largely superior with respect to other more simplifi ed NPZD-like ecosystem models. This is not surprising because these properties of the ecosystem are mostly constrained by large scale features, which are mostly a function of the OGCM resolution common to both NPZD and more complex models.

So, why would it be preferable to use a complex model like PELAGOS for Earth System models and climate change analyses? The most obvious justifi cation is that the different functional groups have different biogeochemical roles in the global carbon cycle and the carbon pathways need to be carefully resolved, which NPZD

models, not carrying C explicitely as state variable, cannot do. In addition, PELAGOS does not implicitely assume a spatial separation between the productive euphotic communities and the purely heterotrophic consumers. Both terms are computed simoultaneosly at each depth, which is an advantage when assessing the biological fate of organic carbon in the mesopelagic and deeper layers for direct estimates of oceanic carbon sequestration pathways (Del Giorgio and Duarte, 2002). Indeed, the model has shown skill in reproducing the spatial distribution and temporal succession of the major LFGs, but still the description of their ecological behavior is crude and the results of long-term climate studies have to be considered as preliminary. This type of prediction is indeed uncertain, but it is important that it is at least based on the application of well-understood biological processes. Purely empirical models can be tuned to a particular observed condition but cannot be relied upon to give a realistic response of the biological system to physical conditions different from the tuning dataset. In this context, a generic deterministic biogeochemistry model is more uncertain in terms of formulations and parameter values but it is much more likely to provide insights into system behavior, especially when the model fails to reproduce observed features in some of the biogeochemical provinces, while doing well in others.

We believe that the strength of our approach is not the separation into different functional groups, but the direct parameterization of the LFGs physiological response to environmental conditions and their changes. The model at this stage has first-order implementations of these mechanisms, which, given the results presented in this paper, are already sufficient for preliminary applications with coupled climate models. At the same time, more sophisticated acclimation/adaptation mechanisms, such as the parameterization of differential size-distributions and explicit allometric control of physiological rates, need to be investigated at the regional scale and then verified in global ocean implementations. These mechanisms represent in fact a way to express some of the plasticity of biological processes in deterministic models.

Acknowledgements

We thank the Goddard Space Flight Center DAAC for SeaWiFS and CZCS satellite data and Yves Dandonneau for the GeP&CO pigment data and methodological explanations. We also acknowledge the availability of data from the US and International JGOFS websites and from the World Ocean Database. We aknowledge the support by the EU projects ENSAMBLES [project no. GOCE-CT-2003-505539] and DYNAMITE [project no. 00393(GOCE)]. We thank Job Baretta and the anonymous reviewers for their critical comments, which helped us to improve the manuscript.

References

Alvain, S., Moulin, C., Dandonneau, Y., Breon, F. M., 2005. Remote sensing of phytoplankton groups in case 1 waters from global SeaWiFS imagery. Deep-Sea Res. Pt. I 52, 1989–2004.

Anderson, T. R., 2005. Plankton functional type modelling: running before we can walk? J. Plankt. Res. 27, 1073–1081.

Aumont, O., Maier-Reimer, E., Monfray, P., Blain, S., 2003. An ecosystem model of the global ocean including Fe, Si, P co-limitations. Glob. Biogeochem. Cy. 17 (2), 1060.

Banse, K., 1987. Seasonality of phytoplankton chlorophyll in the central and northern Arabian Sea. Deep-Sea Res. Pt. II 34, 713–723.

Baretta, J., Ebenhöh, W., Ruardij, P., 1995. The European Regional Seas Ecosystem Model, a complex marine ecosystem model. J. Sea Res. 33 (3-4), 233–246.

Baretta-Bekker, J., Baretta, J., Ebenhoeh, W., 1997. Microbial dynamics in the marine ecosystem model ERSEM II with decoupled carbon assimilation and nutrient uptake. J. Sea Res. 38 (3/4), 195–212.

Baretta-Bekker, J., Baretta, J., Rasmussen, E., 1995. The microbial food web in the European Regional Seas Ecosystem Model. J. Sea Res. 33 (3-4), 363–379.

Behrenfeld, M., Falkowski, P., January 1997. Photosynthetic rates derived from satellite-based chlorophyll concentration. Limnol. Oceanogr. 42 (1), 1–20.

Blanke, B., Delecluse, P., 1993. Variability of the tropical atlantic-ocean simulated by a general-circulation model with 2 different mixed-layer physics. J. Phys. Oceanogr. 23, 1363–1388.

Boyd, P. W., Watson, A. J., Law, C. S., Abraham, E. R., Trull, T., Murdoch, R., Bakker, D. C. E., Bowie, A. R., Buesseler, K. O., Chang, H., Charette, M., Croot, P., Downing, K., Frew, R., Gall, M., Hadfi eld, M., Hall, J., Harvey, M., Jameson, G., LaRoche, J., Liddicoat, M., Ling, R., Maldonado, M. T., McKay, R. M., Nodder, S., Pickmere, S., Pridmore, R., Rintoul, S., Safi , K., Sutton, P., Strzepek, R., Tanneberger, K., Turner, S., Waite, A., Zeldis, J., 2000. A mesoscale phytoplankton bloom in the polar Southern Ocean stimulated by iron fertilization. Nature 407, 695–702.

Coale, K. H., Fitzwater, S. E., Gordon, R. M., Johnson, K. S., Barber, R. T., 1996. Control of community growth and export production by upwelled iron in the equatorial Pacifi c ocean. Nature 379, 621–624.

Conkright, M., Garcia, H., O'Brien, T., Locarnini, R., Boyer, T., Stephens, C., Antonov, J., 2002. World Ocean Atlas 2001, Volume 4: Nutrients. Vol. NOAA Atlas NESDIS 52. U.S. Government Printing Offi ce, Washington D.C., cD-ROMs.
URL http://www.nodc.noaa.gov/OC5/WOA01/woa01v4d.pdf

Conkright, M. E., Gregg, W. W., Levitus, S., 2000. Seasonal cycle of phosphate in the open ocean. Deep-Sea Res. Pt. I 47, 159–175.

Dandonneau, Y., Deschamps, P. Y., Nicolas, J. M., Loisel, H., Blanchot, J., Montel, Y., Thieuleux, F., Becu, G., 2004. Seasonal and interannual variability of ocean color and composition of phytoplankton communities in the North At-

lantic, equatorial Pacifi c and South pacifi c. Deep-Sea Res. Pt. II 51, 303–318.
de Boyer Montégut, C., Madec, G., Fischer, A., Lazar, A., Iudicone, D., 2004. Mixed layer depth over the global ocean: an examination of profi le data and a profi le-based climatology. J. Geophys. Res. 109, C12003.
Del Giorgio, P. A., Duarte, C. M., 2002. Respiration in the open ocean. Nature 420, 379–384.
Doney, S. C., Lindsay, K., Caldeira, K., Campin, J. M., Drange, H., Dutay, J. C., Follows, M., Gao, Y., Gnanadesikan, A., Gruber, N., Ishida, A., Joos, F., Madec, G., Maier-reimer, E., Marshall, J. C., Matear, R. J., Monfray, P., Mouchet, A., Najjar, R., Orr, J. C., Plattner, G. K., Sarmiento, J., Schlitzer, R., Slater, R., Totterdell, I. J., Weirig, M. F., Yamanaka, Y., Yool, A., 2004. Evaluating global ocean carbon models: The importance of realistic physics. Glob. Biogeochem. Cy. 18, 3017.
Ducklow, H. W., 2003. Biogeochemical provinces: towards a JGOFS synthesis. In: Fasham, M. (Ed.), Ocean biogeochemistry. Springer.
Elrod, V. A., Berelson, W. M., Coale, K. H., Johnson, K. S., 2004. The flux of iron from continental shelf sediments: A missing source for global budgets. Geophys. Res. Lett. 31, L12307.
Estublier, A., Levy, M., September 2000. Quel schema numerique pour le transport d'organismes biologiques par la circulation oceanique. Tech. rep., Institut Pierre Simon Laplace.
URL http://www.ipsl.jussieu.fr/modelisation/notes_techniques/Estublier_Levy_NPM00.pdf
Fennel, W., Neumann, T., 1996. The mesoscale variability of nutrients and plankton as seen in a coupled model. Germ. J. Hydrog. 48 (1), 49–71.
Fennel, W., Osborn, T., 2005. A unifying framework for marine ecological model comparison. Deep-Sea Res. Pt. II 52, 1344–1357.
Foujols, M., Levy, M., Aumont, O., Madec, G., July 2000. Opa tracer model reference manual, note technique du pole de modelisation. Tech. rep., Institut Pierre Simon Laplace.
URL http://www.lodyc.jussieu.fr/opa/Docu_Free/Doc_models/Do%c_OPA8.1_Tracer.pdf
Froneman, P. W., K., L. R., McQuaid, C. D., 2001. Size-fractionated Primary Production in the South Atlantic and Atlantic Sectors of the Southern Ocean. J. Plankt. Res. 23 (6), 611–622.
Gao, Y., Fan, S. M., Sarmiento, J. L., 2003. Aeolian iron input to the ocean through precipitation scavenging: A modeling perspective and its implication for natural iron fertilization in the ocean. J. Geophys. Res.-atmos 108, 4221.
Garabato, A. C. N., Polzin, K. L., King, B. A., Heywood, K. J., Visbeck, M., 2004. Widespread intense turbulent mixing in the Southern ocean. Science 303, 210–213.
Gent, P. R., McWilliams, J. C., 1990. Isopycnal mixing in ocean circulation models. J. Phys. Oceanogr. 20, 150–155.
Gordon, R. M., Coale, K. H., Johnson, K. S., 1997. Iron distributions in the equatorial Pacifi c: Implications for new production. Limnol. Oceanogr. 42, 419–431.

Gregg, W. W., Ginoux, P., Schopf, P. S., Casey, N. W., 2003. Phytoplankton and iron: validation of a global three-dimensional ocean biogeochemical model. Deep-Sea Res. Pt. II 50, 3143–3169.

Hourdin, F., Armengaud, A., 1999. The use of finite-volume methods for atmospheric advection of tracer species. Part I: test of various formulations in a general circulation model. Mon. Weather Rev. 127, 822–837.

Jeandel, C., Ruiz-pino, D., Gjata, E., Poisson, A., Brunet, C., Charriaud, E., Dehairs, F., Delille, D., Fiala, M., Fravalo, C., Miquel, J. C., Park, H. Y., Pondaven, P., Queguiner, B., Razouls, S., Shauer, B., Treguer, P., 1998. Kerfix, a time-series station in the Southern Ocean: a presentation. J. Mar. Sys. 17, 555–569.

Jeffrey, S., 1997. Application of pigment methods to oceanography. In: Jeffrey, S., Mantoura, R., Wright, S. (Eds.), Phytoplankton pigments in oceanography: guidelines to modern methods. UNESCO Publishing, Paris, pp. 127–166.

Johnson, K. S., Chavez, F. P., Friederich, G. E., 1999. Continental-shelf sediment as a primary source of iron for coastal phytoplankton. Nature 398, 697–700.

Karl, D., Michaels, A., Bergman, B., Capone, D., Carpenter, E., Letelier, R., Lipschultz, F., Paerl, H., Sigman, D., Stal, L., 2002. Dinitrogen fixation in the world's oceans. Biogeochemistry 57-58, 77–98.

Laubscher, R. K., Perissinotto, R., McQuaid, C. D., 1993. Phytoplankton production and biomass at frontal zones in the Atlantic sector of the Southern Ocean. Polar Biol. 13, 471–481.

Le Quéré, C., Harrison, S., Prentice, I., Buitenhuis, E., Aumont, O., Bopp, L., Claustre, H., da Cunha, L. C., Geider, R., Giraud, X., Klaas, C., Kohfeld, K., Legendre, L., Manizza, M., Platt, T., Rivkin, R., Sathyendranath, S., Uitz, J., Watson, A., Wolf-Gladrow, D., 2005. Ecosystem dynamics based on plankton functional types for global ocean biogeochemistry models. Glob. Change Biol. 11, 2016–2040.

Legendre, L., Rassoulzadegan, F., 1995. Plankton and nutrient dynamics in marine waters. Ophelia 41, 153–172.

Levy, M., Estublier, A., Madec, G., 2001. Choice of an advection scheme for biogeochemical models. Geophys. Res. Lett. 28, 3725–3728.

Longhurst, A. R., 1998. Ecological geography of the sea. Academic Press, San Diego, London.

Mackey, D. J., O'sullivan, J. E., Watson, R. J., 2002. Iron in the western Pacific: a riverine or hydrothermal source for iron in the Equatorial undercurrent? Deep-Sea Res. Pt. II 49, 877–893.

Madec, G., Delecluse, P., Imbard, M., Levy, C., February 1999. OPA8.1 ocean general circulation model reference manual. Notes du pole de modelisation, IPSL, France, http://www.lodyc.jussieu.fr/opa.
URL `http://www.lodyc.jussieu.fr/opa`

Madec, G., Imbard, M., 1996. A global ocean mesh to overcome the North Pole singularity. Clim. Dynam. 12, 381–388.

Manizza, M., Le Quéré, C., Watson, A. J., Buitenhuis, E. T., 2005. Bio-optical feedbacks among phytoplankton, upper ocean physics and sea-ice in a global model. Geophys. Res. Lett. 32, 05603.

Martin, J., Fitzwater, S., 1988. Iron deficiency limits phytoplankton growth in the north-east Pacific subarctic. Nature 331, 341–343.

Martin, J. H., Coale, K. H., Johnson, K. S., Fitzwater, S. E., Gordon, R. M., Tanner, S. J., Hunter, C. N., Elrod, V. A., Nowicki, J. L., Coley, T. L., Barber, R. T., Lindley, S., Watson, A. J., Vanscoy, K., Law, C. S., Liddicoat, M. I., Ling, R., Stanton, T., Stockel, J., Collins, C., Anderson, A., Bidigare, R., Ondrusek, M., Latasa, M., Millero, F. J., Lee, K., Yao, W., Zhang, J. Z., Friederich, G., Sakamoto, C., Chavez, F., Buck, K., Kolber, Z., Greene, R., Falkowski, P., Chisholm, S. W., Hoge, F., Swift, R., Yungel, J., Turner, S., Nightingale, P., Hatton, A., Liss, P., Tindale, N. W., 1994. Testing the iron hypothesis in ecosystems of the equatorial Pacific Ocean. Nature 371, 123–129.

Martin, J. H., Gordon, R. M., Fitzwater, S. E., 1991. The case for iron. Limnol. Oceanogr. 36, 1793–1802.

Michaels, A., Knap, A., 1996. Overview of the U.S. JGOFS Bermuda Atlantic Time Series study. Deep-Sea Res. Pt. II 43, 157–198.

Moore, J. K., Doney, S. C., Glover, D. M., Fung, I. Y., 2002a. Iron cycling and nutrient-limitation patterns in surface waters of the World ocean. Deep-Sea Res. Pt. II 49, 463–507.

Moore, J. K., Doney, S. C., Kleypas, J. A., Glover, D. M., Fung, I. Y., 2002b. An intermediate complexity marine ecosystem model for the global domain. Deep-Sea Res. Pt. II 49, 403–462.

Moore, J. K., Doney, S. C., Lindsay, K., 2004. Upper ocean ecosystem dynamics and iron cycling in a global three-dimensional model. Glob. Biogeochem. Cy. 18, 4028.

Partensky, F., Hess, W. R., Vaulot, D., 1999. Prochlorococcus, a marine photosynthetic prokaryote of global significance. Microbiol. Mol. Biol. Rev. 63, 106–127.

Pondaven, P., Ruiz-pino, D., Fravalo, C., Treguer, P., Jeandel, C., 2000. Interannual variability of Si and N cycles at the time-series station KERFIX between 1990 and 1995 - A 1-D modelling study. Deep-Sea Res. Pt. I 47, 223–257.

Price, N. M., 2005. The elemental stoichiometry and composition of an iron-limited diatom. Limnol. Oceanogr. 50, 1159–1171.

Reynolds, R., 1988. A real-time global sea surface temperature analysis. J. Climate 1, 75–86.

Sarmiento, J. L., Slater, R., Barber, R., Bopp, L., Doney, S. C., Hirst, A. C., Kleypas, J., Matear, R., Mikolajewicz, U., Monfray, P., Soldatov, V., Spall, S. A., Stouffer, R., 2004. Response of ocean ecosystems to climate warming. Glob. Biogeochem. Cy. 18, 3003.

Schmittner, A., Oschlies, A., Giraud, X., Eby, M., Simmons, H. L., 2005. A global model of the marine ecosystem for long-term simulations: Sensitivity to ocean mixing, buoyancy forcing, particle sinking, and dissolved organic matter cycling. Glob. Biogeochem. Cy. 19, 3004.

Semeneh, M., Dehairs, F., Elskens, M., Baumann, M., Kopczynska, E., Lancelot, C., Goeyens, L., 1998. Nitrogen uptake regime and phytoplankton community structure Atlantic and Indian sectors of the Southern Ocean. J. Mar. Sys. 17, 159–177.

Simmons, A., 2001. Development of the ERA-40 data-assimilation system. In: Workshop on Re-analysis. ECMWF, ECMWF, Reading, UK, pp. 11–30.
URL http://www.ecmwf.int/publications/library/ecpublications/proceedings/ERA40-reanalysis_workshop/index.html

Six, K. D., Maier-Reimer, E., 1996. Effects of plankton dynamics on seasonal carbon fluxes in an ocean general circulation model. Glob. Biogeochem. Cy. 10, 559–583.

Smolarkiewicz, P., 1984. A fully multidimensional positive definite advection transport algorithm with small implicit diffusion. J. Comput. Physics 54, 325–362.

Sunda, W. G., Huntsman, S. A., 1997. Interrelated influence of iron, light and cell size on marine phytoplankton growth. Nature 390, 389–392.

Takeda, S., 1998. Influence of iron availability on nutrient consumption ratio of diatoms in oceanic waters. Nature 393, 774–777.

Tegen, I., Fung, I., 1994. Modeling of mineral dust in the atmosphere - sources, transport, and optical-thickness. J. Geophys. Res.-atmos 99, 22897–22914.

Timmermans, K. R., van der Wagt, B., Veldhuis, M. J. W., Maatman, A., de Baar, H. J. W., 2005. Physiological responses of three species of marine pico-phytoplankton to ammonium, phosphate, iron and light limitation. J. Sea Res. 53, 109–120.

Uppala, S., 2001. ECMWF Re-Analysis 1957-2001, ERA-40. In: Workshop on Re-analysis. ECMWF, ECMWF, Reading, UK, pp. 11–30.
URL http://www.ecmwf.int/publications/library/ecpublications/proceedings/ERA40-reanalysis_workshop/index.html

Vichi, M., Pinardi, N., Masina, S., 2006. A generalized model of pelagic biogeochemistry for the global ocean ecosystem. Part I: theory. J. Mar. Sys. XX, xxx–xxx, in press.

Zalesak, S., 1979. Multidimensional flux-corrected transport algorithms for fluids. J. Comput. Physics 31, 335–362.

Name	Description	Physics	Biology
C1	non-local and local terms	$-\mathbf{u}_H \cdot \nabla_H C + \nabla_H \cdot (A_H \cdot \nabla_H C) - w\frac{\partial C}{\partial z} + \frac{\partial}{\partial z} A_V \frac{\partial C}{\partial z}$	$-w_C \frac{\partial C}{\partial z} + \left.\frac{\partial C}{\partial t}\right\|_{bio}$
C2	local terms only	$-w\frac{\partial C}{\partial z} + \frac{\partial}{\partial z} A_V \frac{\partial C}{\partial z}$	$-w_C \frac{\partial C}{\partial z} + \left.\frac{\partial C}{\partial t}\right\|_{bio}$
C3	vertical turbulence only	$\frac{\partial}{\partial z} A_V \frac{\partial C}{\partial z}$	$-w_C \frac{\partial C}{\partial z} + \left.\frac{\partial C}{\partial t}\right\|_{bio}$

Table 1
List of experiments with different configurations of the physical terms solved in eq. (1).

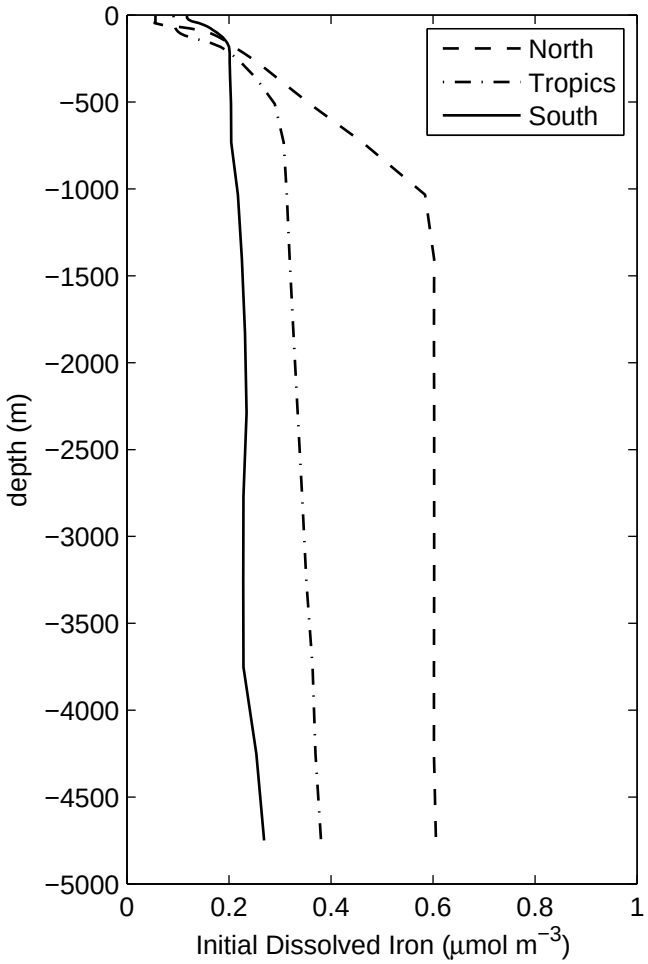

Figure 1. Initial profiles of dissolved iron prescribed in three zonal bands (north hemisphere, tropical regions, Southern Ocean).

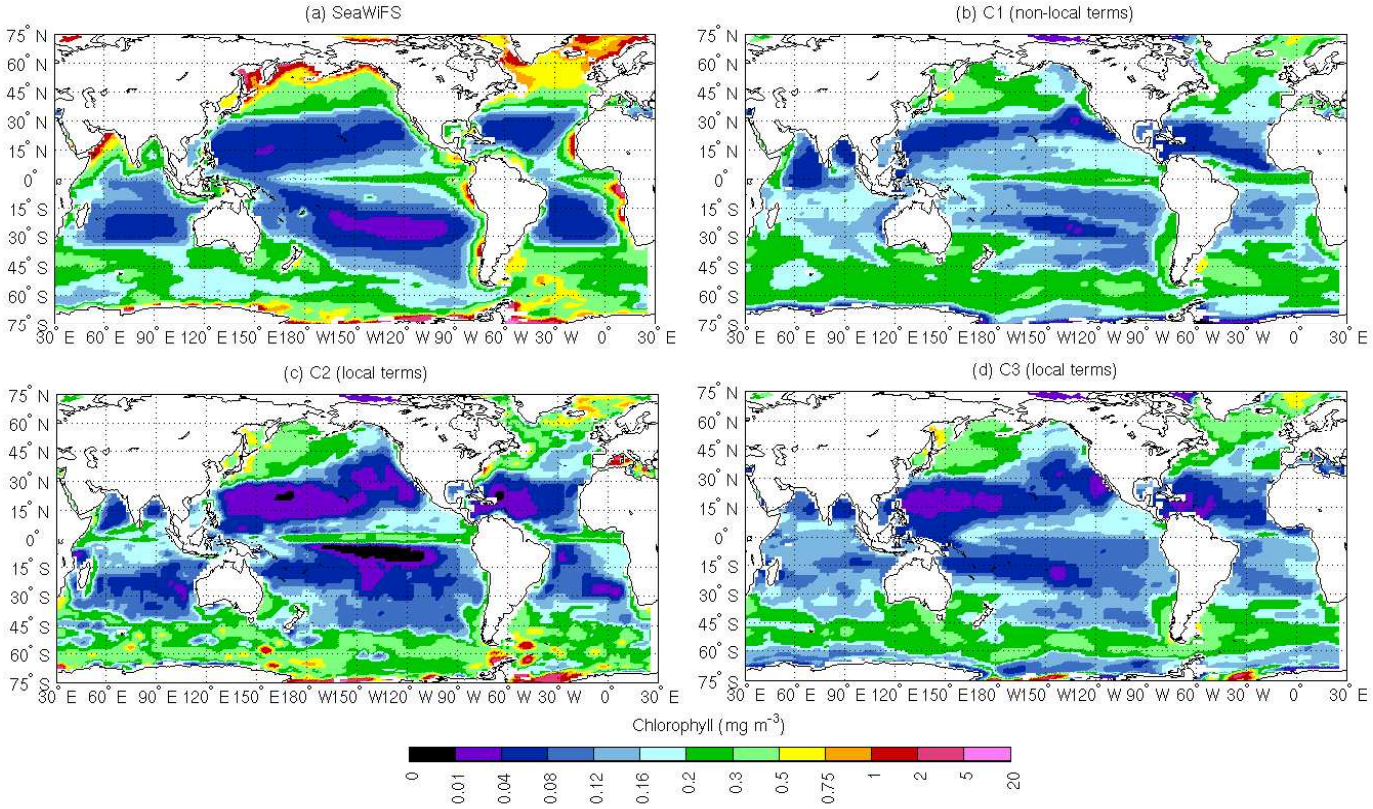

Figure 2. Annual chl maps. a) SeaWiFS average (SMI, 1998-2003); b) run C1 with all the advection-diffusion-reaction terms; c) run C2 with horizontal advection and diffusion terms neglected; d) run C3, with only vertical diffusive and reaction terms (see Table 1).

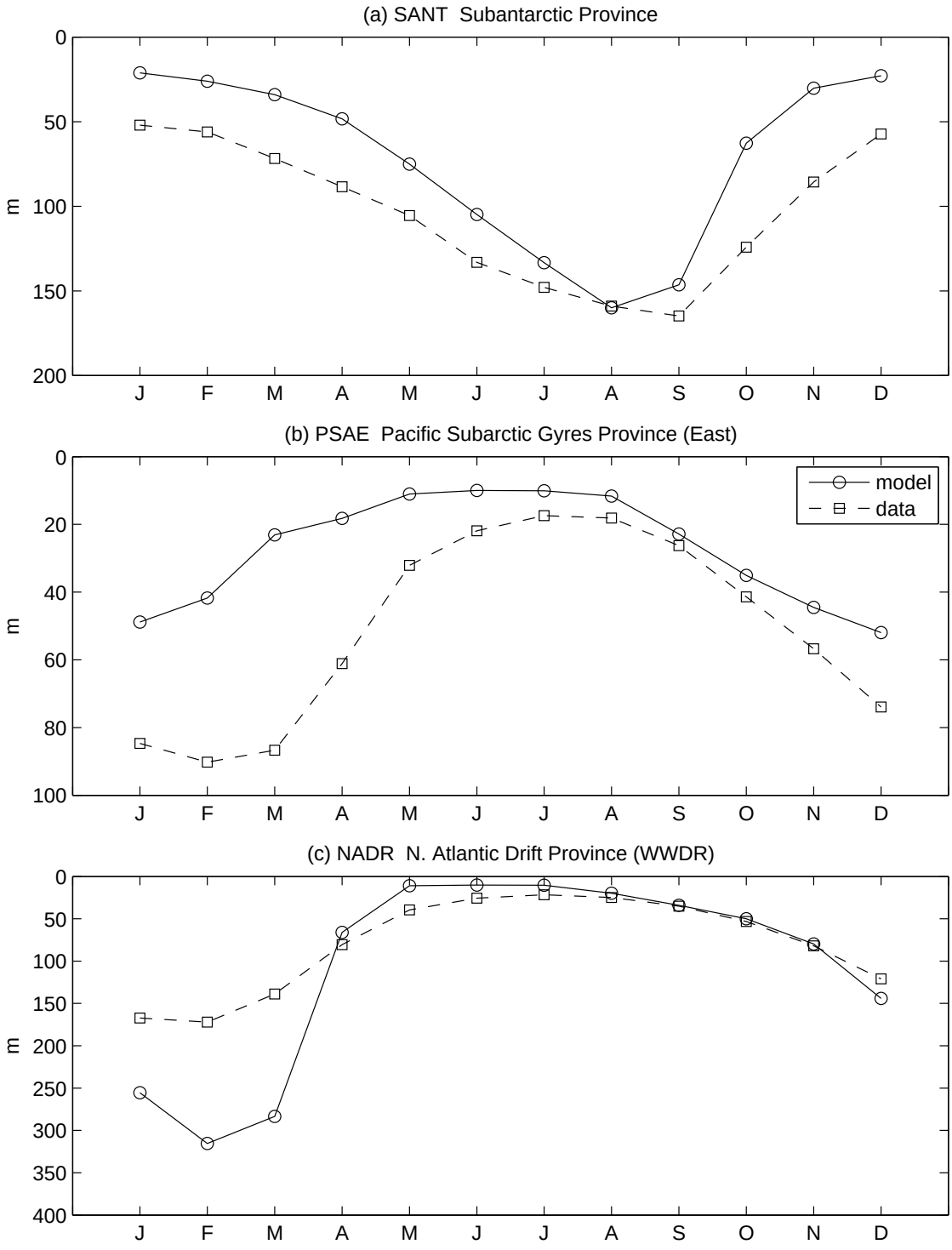

Figure 3. Monthly means of mixed layer depths from model results and from the climatology of de Boyer Montégut et al. (2004) in a) Sub-Antarctic province (SANT), b) Pacific Sub-Arctic Eastern Province (PSAE) and c) North Atlantic Drift province (NADR).

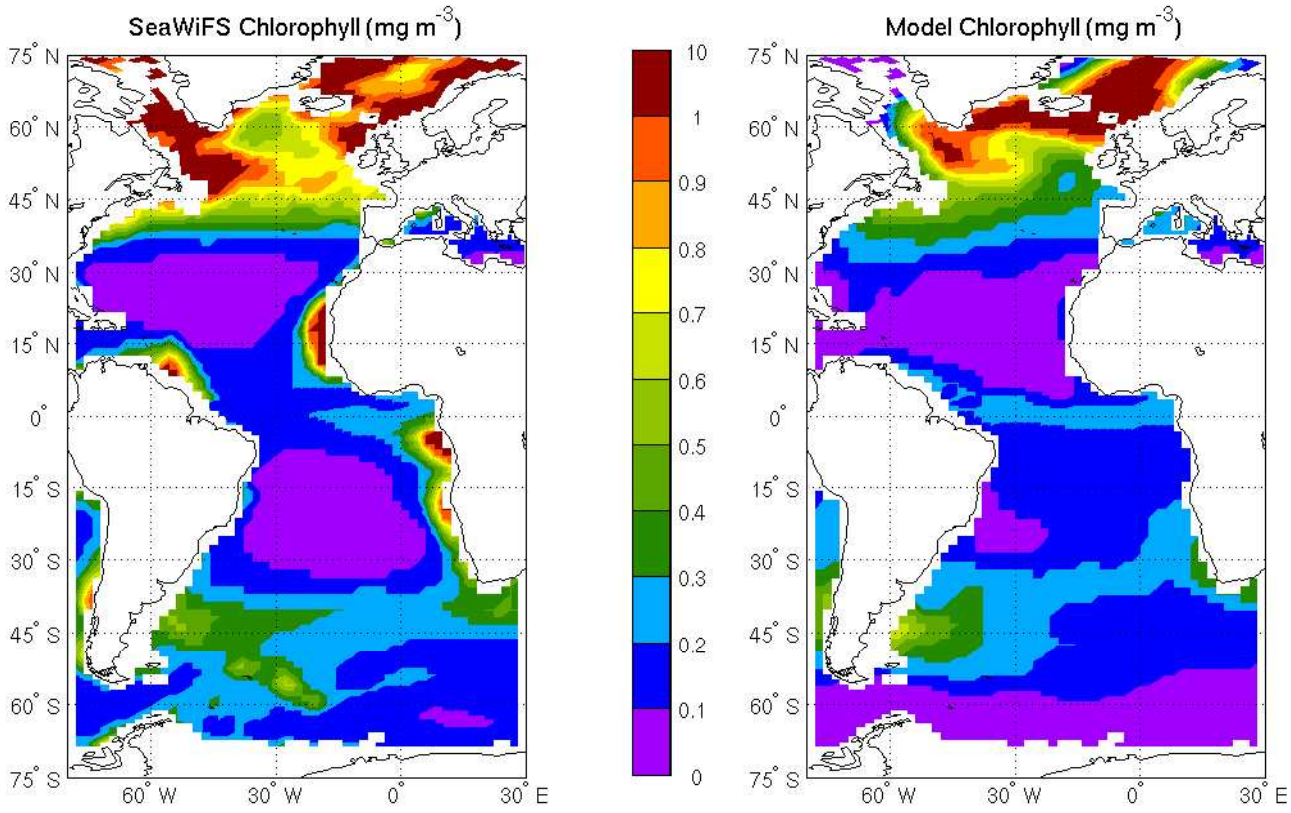

Figure 4. Mean chlorophyll concentration from (a) SeaWiFS and (b) model during boreal spring (AMJ) in the Atlantic Ocean.

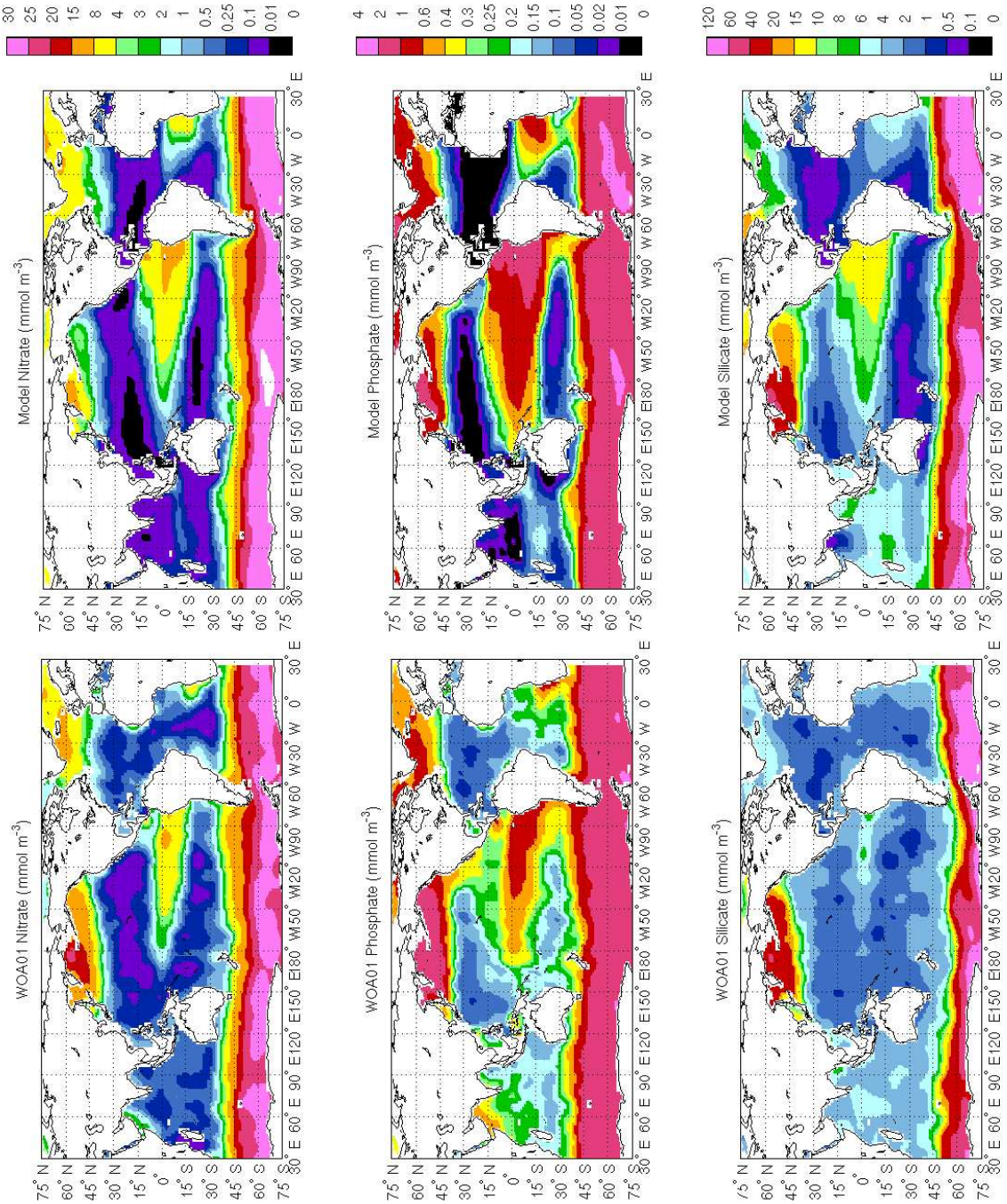

Figure 5. Annual means of simulated surface nutrient concentrations from run C1 for nitrate, phosphate and silicate, and WOA01 climatology.

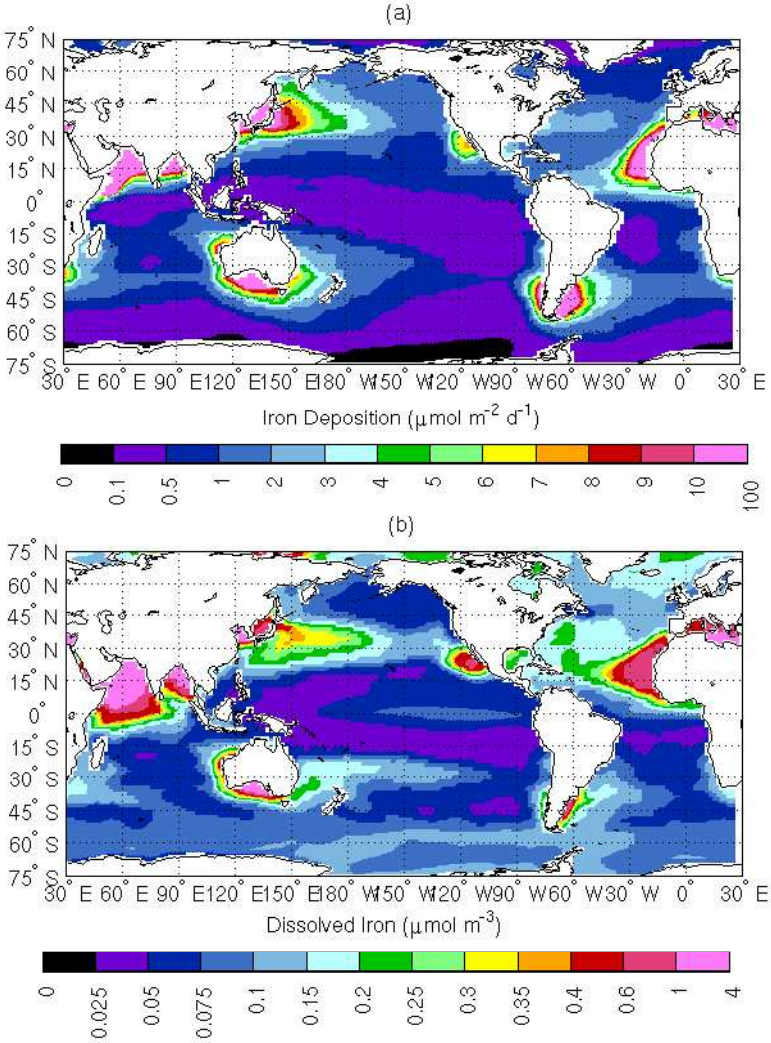

Figure 6. Annual means of (a) iron dust deposition forcing flux from Tegen and Fung (1994) and (b) surface dissolved Fe concentration from C1 simulation.

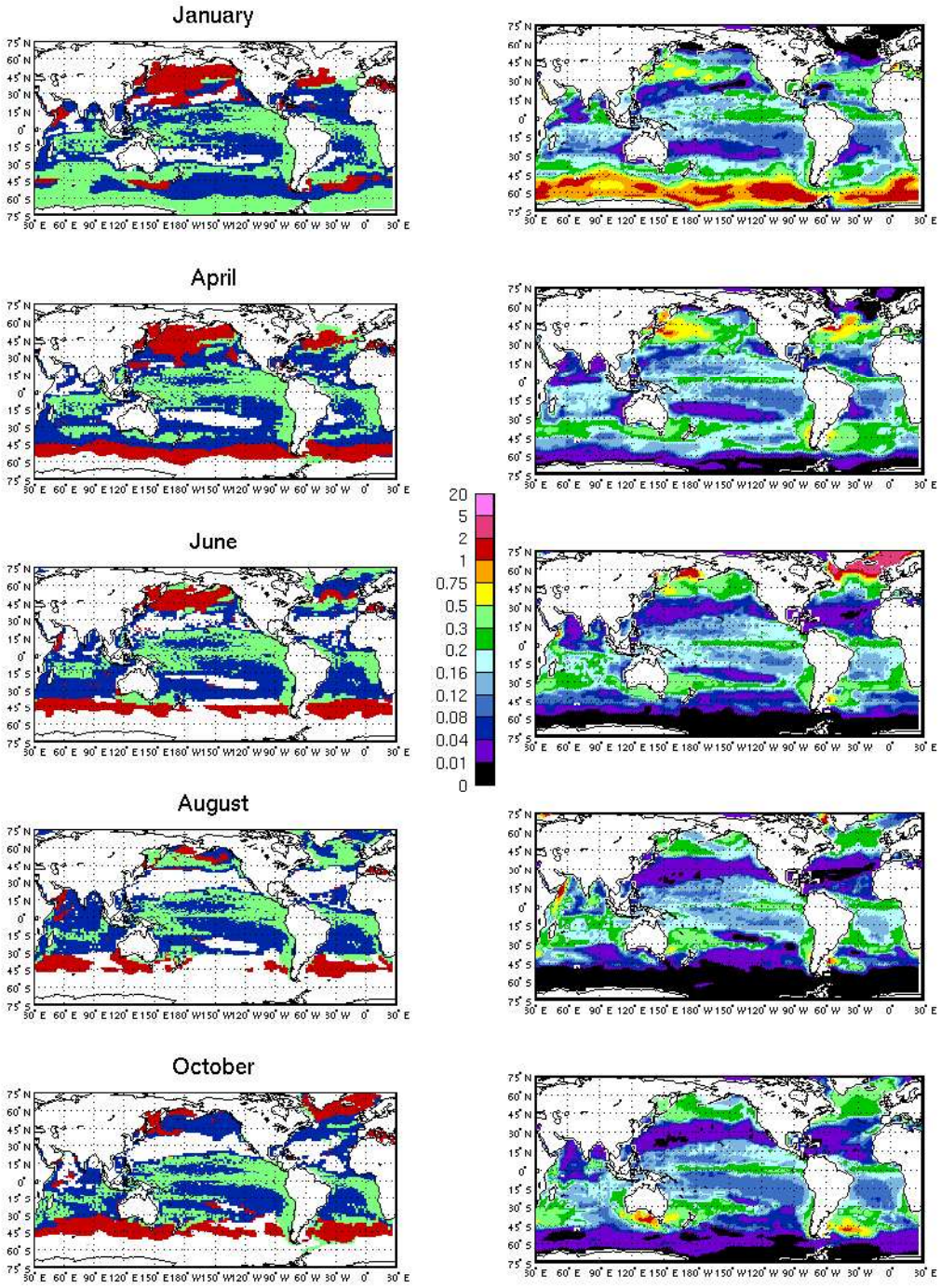

Figure 7. Monthly means of phytoplankton groups distribution (left panels, red = diatoms, blue = nanophytoplankton, green = picophytoplankton) and simulated satellite chl for January, April, June, August and October from run C1. The figure can be compared with satellite-based estimates by Alvain et al. (2005).

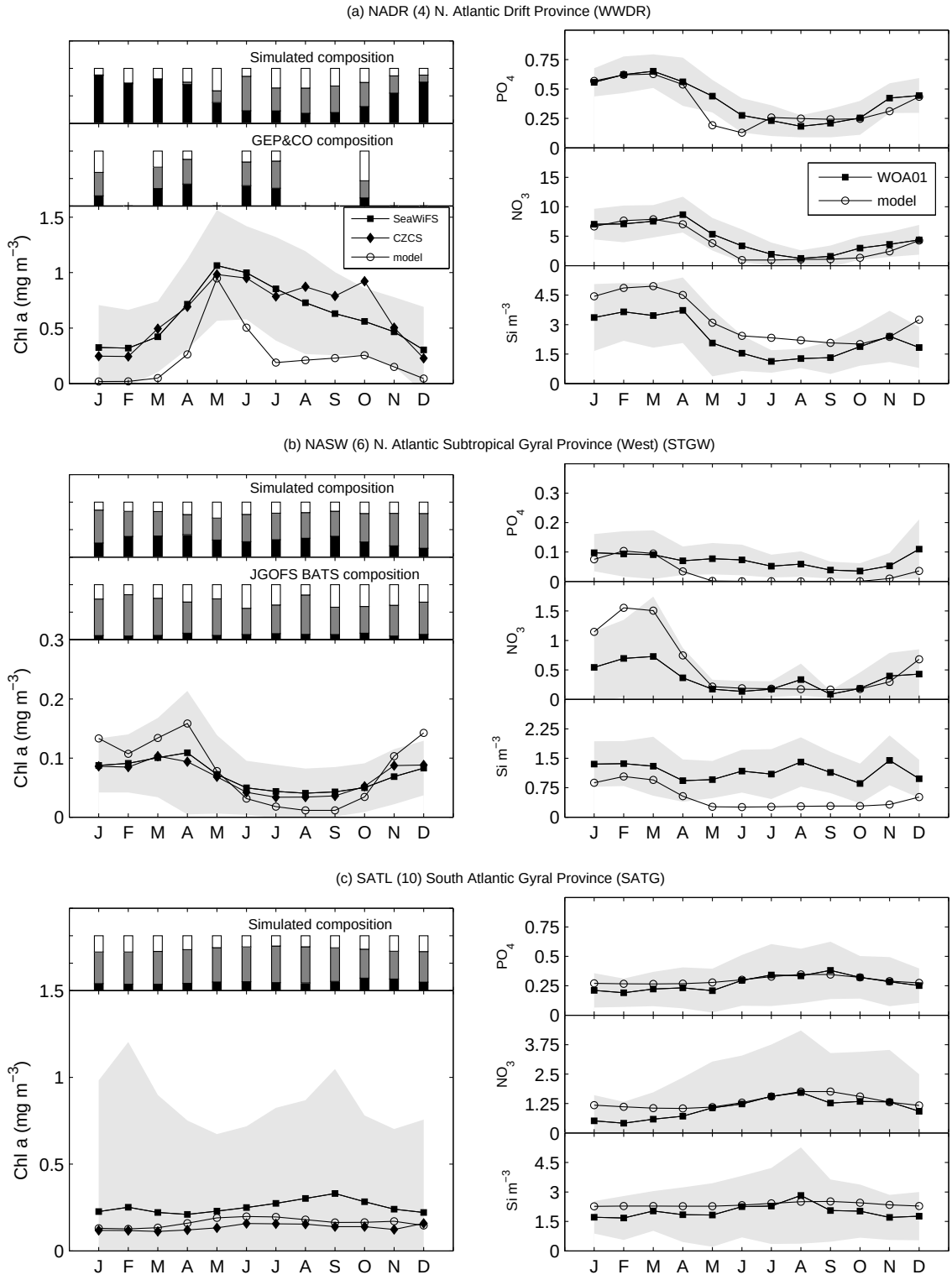

Figure 8. Seasonal evolution of surface chlorophyll and phytoplankton composition (left) and nutrient concentrations (right; phosphate, nitrate and silicate for each panel), averaged over the selected Atlantic biogeochemical provinces (a) NADR, (b) NASW and (c) SATL. Simulation results are compared with data from CZCS, SeaWiFS and WOA01 averaged over the same spatial domains. The gray-shaded area is the spatial standard deviation of SeaWiFS and WOA01 data. Bars represent the relative percentage of phytoplankton functional groups during each month (black=diatoms; gray=nano; white=pico).

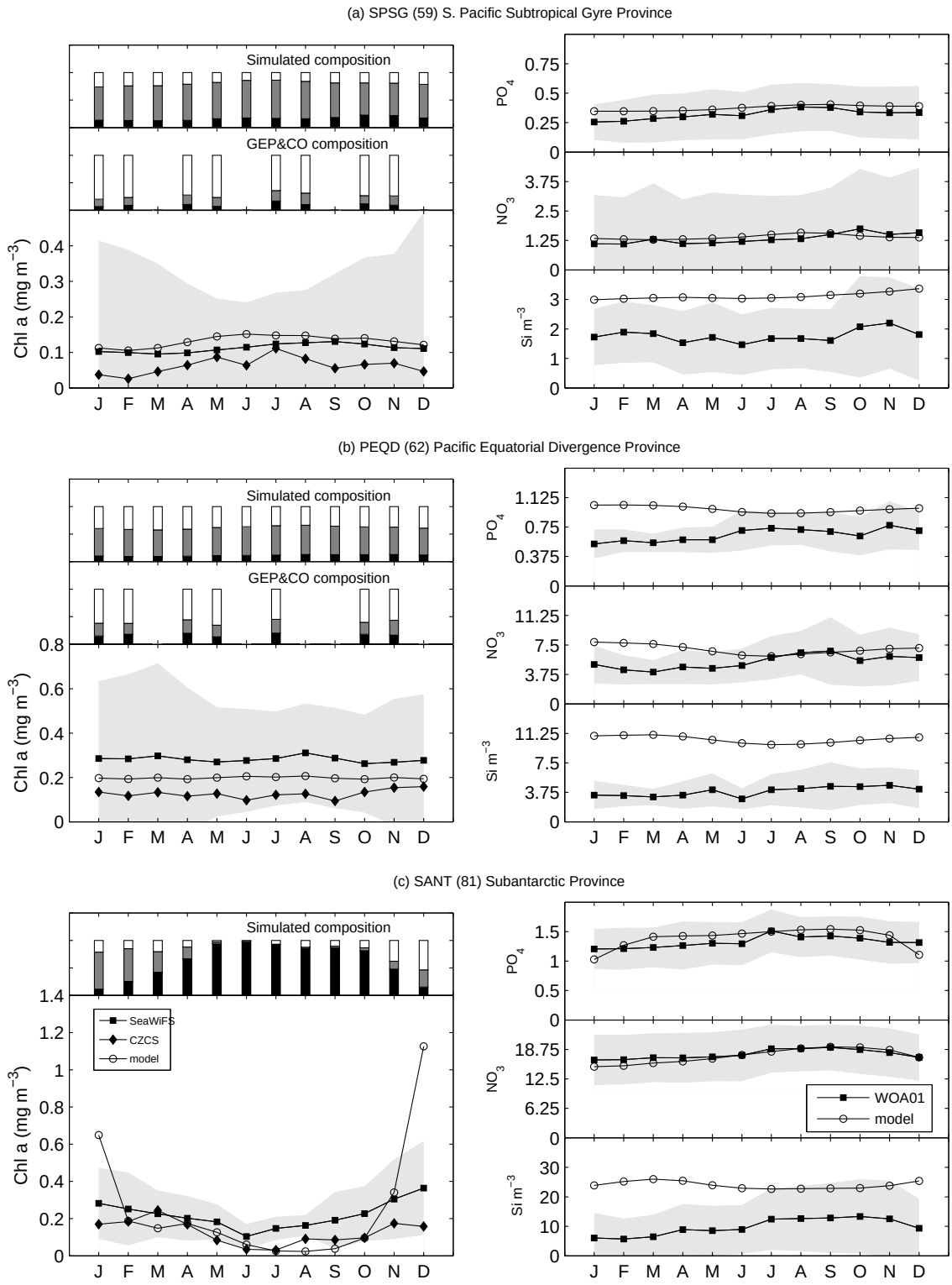

Figure 9. Seasonal evolution of surface chlorophyll and phytoplankton composition (left) and nutrient concentrations (right; phosphate, nitrate and silicate for each panel), averaged over the selected Pacific biogeochemical provinces (a) SPSG, (b) PEQD and Southern Ocean SANT (c). Simulation results are compared with data from CZCS, SeaWiFS and WOA01 averaged over the same spatial domains. The gray-shaded area is the spatial standard deviation of SeaWiFS and WOA01 data. Histograms represent the relative percentage of phytoplankton functional groups during each month (black=diatoms; gray=nano; white=pico).

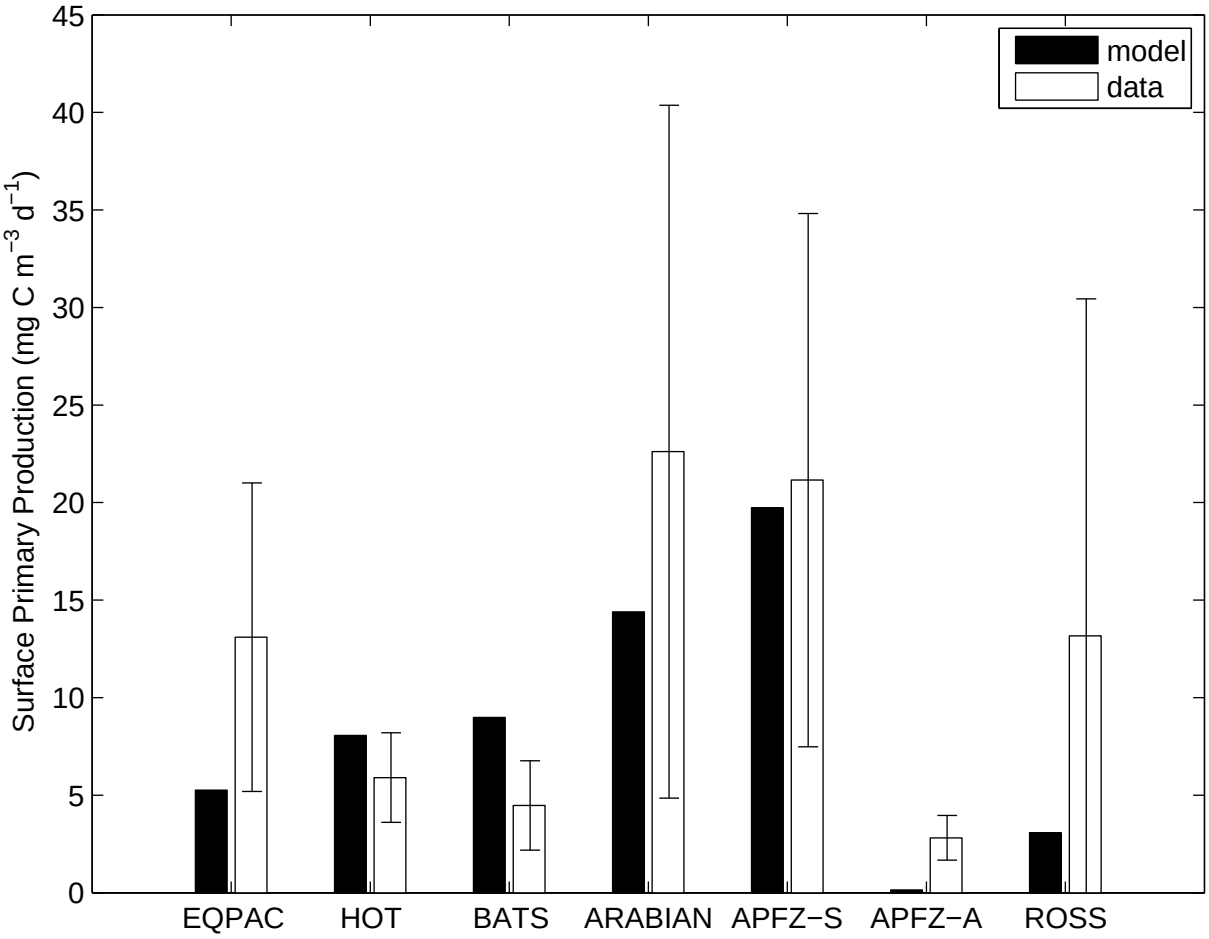

Figure 10. Comparison of modeled and observed mean surface primary production at JGOFS study sites. EQPAC = Eastern Equatorial Pacific (12°S-12°N, 140°W, Feb 1992 - Dec 1992); HOT = Hawaiian Ocean Times-series (22°45'N, 158°W, Oct 1988 - Dec 1998); BATS = Bermuda Atlantic Time-series (31°40'N, 64°10'W, Oct 1988 - Dec 1999); ARABIAN = Arabian Sea (10-23°N, 57-69°E, Jan 1995 - Dec 1995); APFZ = Antarctic Polar Front Zone (60-70°S, 165-175°W, APFZ-S=Dec 1997, APFZ-A=Mar-Apr 1998); ROSS = Ross Sea (70-76°S, 168-175°W, Spring-Summer 1996-98). Bars represent the standard deviation of the sample.

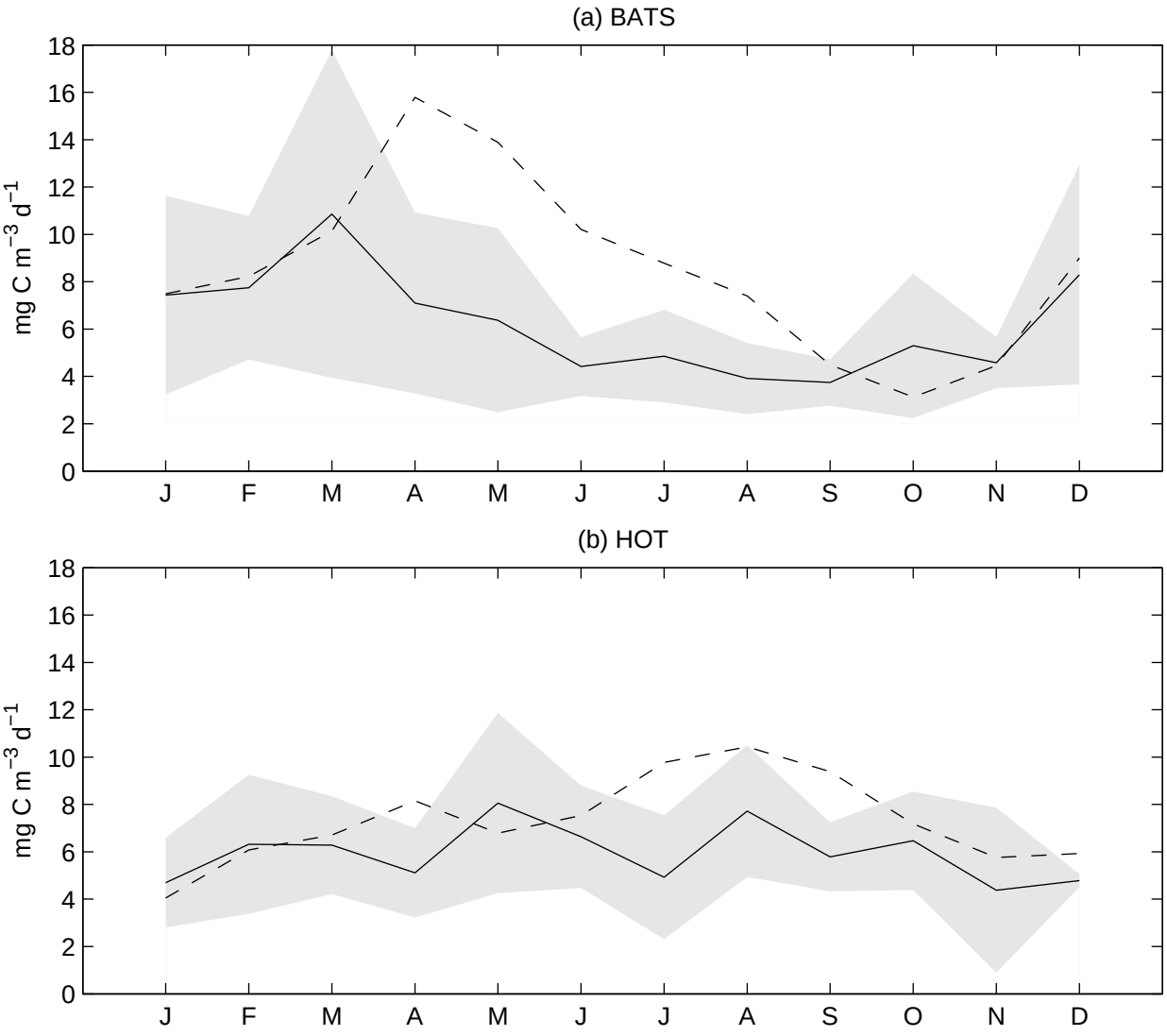

Figure 11. Seasonal cycles of observed (continuous line) and simulated (dashed line) gross primary production rates (monthly means averaged in the mixed layer) at (a) the Bermuda Atlantic TimeSeries and (b) the Hawaii Ocean Timeseries. Grey shading is the standard deviation of the 10 years data sample.